

Efficient and Degree-Guided Graph Generation via Discrete Diffusion Modeling

Xiaohui Chen¹ Jiaxing He¹ Xu Han¹ Li-Ping Liu¹

Abstract

Diffusion-based generative graph models have been proven effective in generating high-quality small graphs. However, they need to be more scalable for generating large graphs containing thousands of nodes desiring graph statistics. In this work, we propose EDGE, a new diffusion-based generative graph model that addresses generative tasks with large graphs. To improve computation efficiency, we encourage graph sparsity by using a discrete diffusion process that randomly removes edges at each time step and finally obtains an empty graph. EDGE only focuses on a portion of nodes in the graph at each denoising step. It makes much fewer edge predictions than previous diffusion-based models. Moreover, EDGE admits explicitly modeling the node degrees of the graphs, further improving the model performance. The empirical study shows that EDGE is much more efficient than competing methods and can generate large graphs with thousands of nodes. It also outperforms baseline models in generation quality: graphs generated by our approach have more similar graph statistics to those of the training graphs.

1. Introduction

There is a long history of using random graph models (Newman et al., 2002) to model large graphs. Traditional models such as Erdős-Rényi (ER) model (Erdos et al., 1960), Stochastic-Block Model (SBM) (Holland et al., 1983), and Exponential-family Random Graph Mdoels (Lusher et al., 2013) are often used to model existing graph data and focus on prescribed graph structures. Besides modeling existing data, the interesting problem is to generate new graphs to simulate existing ones (Ying & Wu, 2009), which has applications such as network data sharing. In generative tasks (Chakrabarti & Faloutsos, 2006), traditional models often fall short in describing complex structures. A promising direction is to use deep neural models to generate large graphs.

¹Department of Computer Science, Tufts University, Medford, MA, USA. Correspondence to: Xiaohui Chen <xiaohui.chen@tufts.edu>, Li-Ping Liu <liping.liu@tufts.edu>.

Proceedings of the 40th International Conference on Machine Learning, Honolulu, Hawaii, USA. PMLR 202, 2023. Copyright 2023 by the author(s).

There are only a few deep generative models designed for generating large graphs. NetGAN and its variants (Bojchevski et al., 2018; Rendsburg et al., 2020) are designed to generate large graphs. However, recent research (Broido & Clauset, 2019; Seshadhri et al., 2020; Chanpuriya et al., 2021) has highlighted the limitations of these models in accurately reproducing desired statistics of the target graph, such as triangle counts and clustering coefficient.

These models generate a graph in multiple steps and are NOT edge-independent because edges generated in later steps depend on previously generated edges. There are also more flexible than models (Kipf & Welling, 2016b; Madhawa et al., 2019; Lippe & Gavves, 2020) that directly predict an adjacency matrix in one step. They also have an advantage over auto-regressive graph models (You et al., 2018; Liao et al., 2019) as they are invariant to node permutations and can better capture global graph structures. However, diffusion-based models are only designed for tasks with small graphs (usually less than one hundred nodes).

Diffusion-based generative models (Liu et al., 2019; Niu et al., 2020; Jo et al., 2022; Chen et al., 2022b) have been proven successful in modeling small graphs. These models generate a graph in multiple steps and are NOT edge-independent because edges generated in later steps depend on previously generated edges. There are also more flexible than models (Kipf & Welling, 2016b; Madhawa et al., 2019; Lippe & Gavves, 2020) that directly predict an adjacency matrix in one step. They also have an advantage over auto-regressive graph models (You et al., 2018; Liao et al., 2019) as they are invariant to node permutations and can better capture global graph structures. However, diffusion-based models are only designed for tasks with small graphs (usually less than one hundred nodes).

This work aims to scale diffusion-based graph models to generate large graphs. The major scalability issue of diffusion-based models is that they must compute a latent vector or a probability for each node pair in a graph at each diffusion step (Niu et al., 2020; Jo et al., 2022) – the computation cost is $O(TN^2)$ if the model generates a graph with N nodes using T steps. The learning task becomes challenging when the graphs are large. Moreover, without explicit specification, these models often cannot capture global graph statis-

tics such as clustering coefficients. As a result, the model performance degrades when the graphs’ size scales up.

We propose *Efficient Degree-guided graph GEnenerative model* (EDGE) based on a discrete diffusion process. There are three innovations in the development of EDGE. First, we encourage the sparsity of graphs in the diffusion process by setting empty graphs as the convergent distribution. The diffusion process we considered can be viewed as an edge-removal process. Since we parameterize the denoising network with a message-passing neural network (MPNN) (Kipf & Welling, 2016a), whose runtime is linear in the number of edges, the sparsity in graphs dramatically reduces the computation. Second, the denoising network is designed to only predict edges for a few “active nodes” that possibly have edge changes for each denoising step. This strategy dramatically decreases the number of predictions and the computation time. More importantly, this design is naturally derived from the aforementioned discrete diffusion process without modifying the forward transition distribution. Third, we model the node degrees of the graphs explicitly. By characterizing the node degrees, the statistics of the generated graphs are much closer to the training graphs. While other diffusion-based graph models struggle to even train or sample on large graphs, empirical results demonstrate that our approach can efficiently generate large graphs with desired statistical properties. We summarize our contributions as follows:

- we use empty graphs as the convergent distribution in a discrete diffusion process to reduce computation;
- we propose a new generative process that only predicts edges between a fraction of nodes in graphs;
- we explicitly model node degrees in the probabilistic framework to improve graphs statistics of generated graphs; and
- we conduct an extensive empirical study, which shows that our method can efficiently generate large graphs with desired statistics.

2. Background

This work considers graph generative models that sample adjacency matrices to generate graphs. Denote \mathcal{A}^N the space of adjacency matrices of size N . We consider simple graphs without self-loops or multi-edges, so an adjacency matrix $\mathbf{A} \in \mathcal{A}^N$ is a binary symmetric matrix with a zero diagonal. A generative model defines a distribution over \mathcal{A}^N .

In this work, the construction of a generative model depends on a discrete diffusion process (Austin et al., 2021; Hoogeboom et al., 2021; Vignac et al., 2022). Let \mathbf{A}^0 denote a graph from the data, then the diffusion process defined by $q(\mathbf{A}^t | \mathbf{A}^{t-1})$ corrupts \mathbf{A}^0 in T steps and forms a trajectory

$(\mathbf{A}^0, \mathbf{A}^1, \dots, \mathbf{A}^T)$. We treat $(\mathbf{A}^1, \dots, \mathbf{A}^T)$ as latent variables, then $q(\mathbf{A}^1, \dots, \mathbf{A}^T | \mathbf{A}^0) = \prod_{t=1}^T q(\mathbf{A}^t | \mathbf{A}^{t-1})$. As $T \rightarrow \infty$, $q(\mathbf{A}^T)$ approaches a convergent distribution, often a simple one with easy samples. We often choose a large enough T so that $q(\mathbf{A}^T)$ is a good approximation of the convergent distribution.

By modeling these trajectories with a denoising model $p_\theta(\mathbf{A}^{t-1} | \mathbf{A}^t)$ parameterized by θ , we have a joint model $p_\theta(\mathbf{A}^{0:T}) = p(\mathbf{A}^T) \prod_{t=1}^T p_\theta(\mathbf{A}^{t-1} | \mathbf{A}^t)$, whose marginal $p_\theta(\mathbf{A}^0)$ models the data. Here $p(\mathbf{A}^T)$ is the convergent distribution in q .

Usually, $q(\mathbf{A}^t | \mathbf{A}^{t-1})$ usually needs easy probability calculations. One choice is to treat each edge independently, and

$$q(\mathbf{A}^t | \mathbf{A}^{t-1}) = \prod_{i,j: i < j} \mathcal{B}(\mathbf{A}_{i,j}^t; (1 - \beta_t) \mathbf{A}_{i,j}^{t-1} + \beta_t p) \quad (1)$$

$$:= \mathcal{B}(\mathbf{A}^t; (1 - \beta_t) \mathbf{A}^{t-1} + \beta_t p).$$

Here $\mathcal{B}(x; \mu)$ represents the Bernoulli distribution over x with Bernoulli parameter μ . We also use $\mathcal{B}(\mathbf{A}; \mu)$ to represent the probability of independent Bernoulli variables arranged in a matrix. The diffusion rate β_t determines the probability of resampling from the Bernoulli distribution, whose parameter is p .

This diffusion process requires two special properties for model fitting. First, we can sample \mathbf{A}^t at any timestep t directly from \mathbf{A}^0 . Let $\alpha_t = 1 - \beta_t$ and $\bar{\alpha}_t = \prod_{\tau=1}^t \alpha_\tau$,

$$q(\mathbf{A}^t | \mathbf{A}^0) = \mathcal{B}(\mathbf{A}^t; \bar{\alpha}_t \mathbf{A}^0 + (1 - \bar{\alpha}_t)p). \quad (2)$$

The diffusion rates β_t -s are defined in a way such that $\bar{\alpha}_T$ is almost 0, then \mathbf{A}^T is almost independent from \mathbf{A}^0 , i.e., $q(\mathbf{A}^T | \mathbf{A}^0) \approx p(\mathbf{A}^T) \equiv \mathcal{B}(\mathbf{A}^T; p)$. The configuration of β_t -s is called *noise scheduling*. In the context of graph generation, the binomial distribution $p(\mathbf{A}^T)$ is approximately the Erdős-Rényi graph model $G(N, p)$ (Erdos et al., 1960), with p being the probability of forming an edge between any two nodes.

Second, we can compute the posterior of the forward transition when conditioning on \mathbf{A}^0 :

$$q(\mathbf{A}^{t-1} | \mathbf{A}^t, \mathbf{A}^0) = \frac{q(\mathbf{A}^t | \mathbf{A}^{t-1}) q(\mathbf{A}^{t-1} | \mathbf{A}^0)}{q(\mathbf{A}^t | \mathbf{A}^0)}. \quad (3)$$

Since all the terms on the right-hand side are known, the posterior can be computed analytically.

The generative model $p_\theta(\mathbf{A}^{0:T})$ is trained by maximizing a variational lower bound of $\log p_\theta(\mathbf{A}^0)$ (Ho et al., 2020; Hoogeboom et al., 2021; Austin et al., 2021). In an intuitive understanding, $p_\theta(\mathbf{A}^{t-1} | \mathbf{A}^t)$ is learned to match the posterior of the forward transition $q(\mathbf{A}^{t-1} | \mathbf{A}^t, \mathbf{A}^0)$.

During generation, we sample $\mathbf{A}^T \sim p(\mathbf{A}^T)$ and then “denoise” it iteratively with $p_\theta(\mathbf{A}^{t-1} | \mathbf{A}^t)$ to get an \mathbf{A}^0 sample.

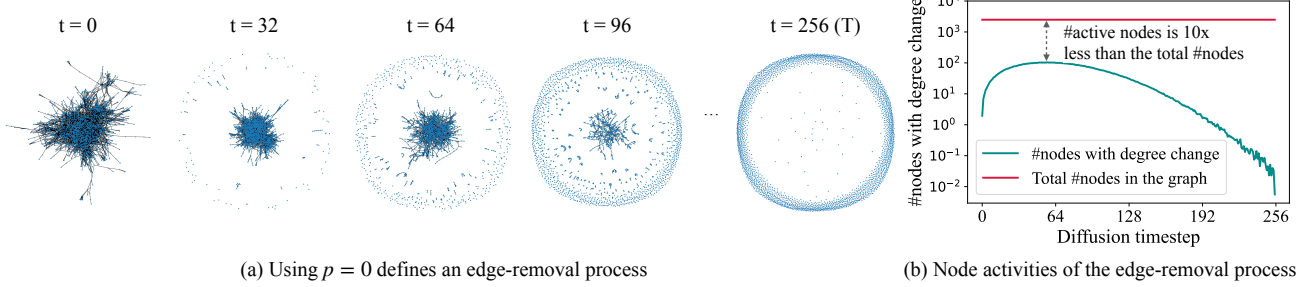


Figure 1. Dynamic of discrete diffusion process using $p = 0$ and its nodes behavior for the Cora dataset: (a) the diffusion process defined by setting $p = 0$ is an edge-removal process. The reverse of it is to construct a graph by gradually adding edges starting from an empty graph. (b) under linear noise scheduling, the number of nodes that have their edges removed (active nodes) at each timestep is less than the total number of nodes in the graph by at least one order of magnitude.

3. EDGE: Efficient and Degree-guided Graph Generation

3.1. Diffuse graphs to empty graphs – a motivation

With the main purpose of computation efficiency, we advocate setting $p = 0$ and using $G(N, 0)$ as the convergent distribution. This configuration improves the sparsity of the adjacency matrices in diffusion trajectories, thus reducing computation. We consider the amount of computation in the denoising model $p_\theta(\mathbf{A}^{t-1}|\mathbf{A}^t)$ from two aspects: the computation on the input \mathbf{A}^t and the number of entries to be predicted in the output \mathbf{A}^{t-1} .

We first consider the computation on the input side. We assume that the denoising model $p_\theta(\mathbf{A}^{t-1}|\mathbf{A}^t)$ is constructed with an MPNN. Suppose the input graph \mathbf{A}^t has M^t edges, and we treat hidden dimensions and the number of network layers as constants. A typical MPNN needs to perform $O(M^t)$ message-passing operations to compute node vectors. The total number of message-passing operations over the trajectory is $O(\sum_{t=1}^T M^t)$. After some calculations, we show that

$$\sum_{t=1}^T M^t = M^0 \sum_{t=1}^T \bar{\alpha}_t + \frac{N(N-1)p}{2} \sum_{t=1}^T 1 - \bar{\alpha}_t. \quad (4)$$

Setting $p = 0$ eliminates the second term and reduces the number of edges in graphs in the diffusion trajectory by a significant factor, then the MPNN will have much fewer message-passing operations.

We then analyze the number of entries we need to predict in the output \mathbf{A}^{t-1} . When $p = 0$, the forward process is an edge-removal process, and the degree of a node is non-increasing for any forward transition. A node with a degree change from $t-1$ to t is considered “active”. When a node is inactive at $t-1$, all edges incident to this node is kept at t . Figure 1 shows the average number of active nodes for each forward transition. We observe that active nodes only take a small fraction of the total when the convergent distribution is $G(N, 0)$. While traditional discrete diffusion

models require predicting all node pairs, such observation indicates that we can save computation by only predicting edges between the active nodes.

In the reverse process, the denoising model must infer which nodes should be added edges for each step before predicting edges. This requires us to reformulate the denoising model to model both the node selection and the edge prediction procedure. From now on, we only consider the diffusion process with $p = 0$.

3.2. A diffusion-based model that explicitly models active nodes

We treat the “active nodes” as latent variables $\mathbf{s}^{1:T}$ and incorporate them into both the forward and reverse processes. Denote $\mathbf{d}^t = \deg(\mathbf{A}^t)$ be the node degree vector of \mathbf{A}^t , then $\mathbf{s}^t := \mathbb{1}[\mathbf{d}^{t-1} \neq \mathbf{d}^t]$ is a binary vector indicating which nodes are active (have degree change) from $t-1$ to t or the other way around. In the following, we redefine the forward and reverse processes. The interpretation of the generative framework is demonstrated in Figure 2.

Forward process. With the introduced latent variables $\mathbf{s}^{1:T}$, we show that the forward process can be rewritten into the following decomposition:

$$q(\mathbf{A}^{1:T}, \mathbf{s}^{1:T} | \mathbf{A}^0) = \prod_{t=1}^T q(\mathbf{A}^t | \mathbf{A}^{t-1}) q(\mathbf{s}^t | \mathbf{A}^{t-1}, \mathbf{A}^t). \quad (5)$$

The forward process does not change by including $\mathbf{s}^{1:T}$. Since the value of \mathbf{s}^t is deterministic given \mathbf{A}^{t-1} and \mathbf{A}^t . This allows us to use still the forward transition $q(\mathbf{A}^t | \mathbf{A}^{t-1})$ to draw the entire sequence.

Reverse process. Since we want to save computation by predicting active nodes during generation, for the reverse process, the denoising model is decomposed into

$$p_\theta(\mathbf{A}^{0:T}, \mathbf{s}^{1:T}) = p(\mathbf{A}^T) \prod_{t=1}^T p_\theta(\mathbf{A}^{t-1} | \mathbf{A}^t, \mathbf{s}^t) p_\theta(\mathbf{s}^t | \mathbf{A}^t). \quad (6)$$

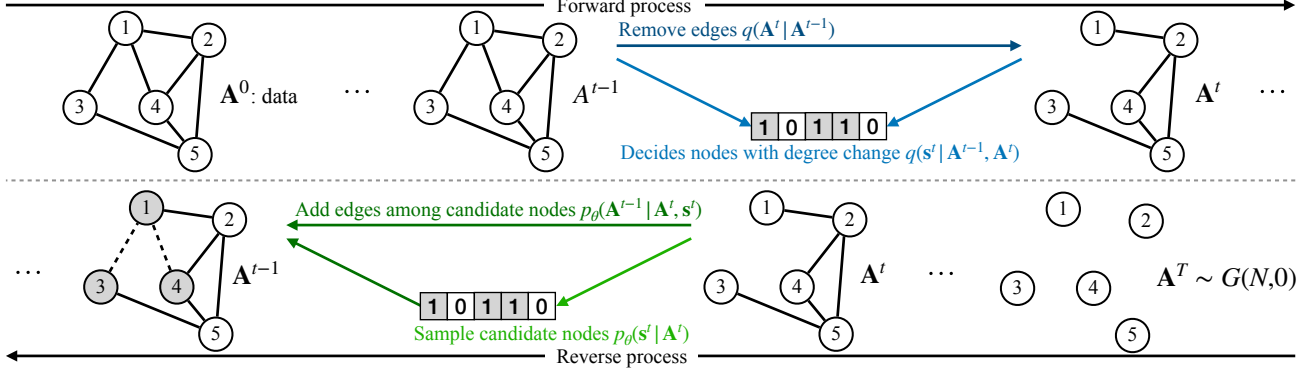


Figure 2. Forward and reverse processes. For the forward process, \mathbf{A}^t is sampled from $q(\mathbf{A}^t | \mathbf{A}^{t-1})$, then \mathbf{s}^t is deterministically generated given \mathbf{A}^{t-1} and \mathbf{A}^t . For the reverse process, \mathbf{s}^t is first sampled from a node selection distribution $p_\theta(\mathbf{s}^t | \mathbf{A}^t)$, then \mathbf{A}^{t-1} is sampled from the parameterized distribution $p_\theta(\mathbf{A}^{t-1} | \mathbf{A}^t, \mathbf{s}^t)$.

Here both $p_\theta(\mathbf{A}^{t-1} | \mathbf{A}^t, \mathbf{s}^t)$ and $p_\theta(\mathbf{s}^t | \mathbf{A}^t)$ are learnable distributions. Intuitively, given \mathbf{A}^t , the denoising model first predicts which nodes are actives (\mathbf{s}^t) and then generates edges between them to obtain \mathbf{A}^{t-1} . Since we only predict edges between nodes indicated by \mathbf{s}^t , all edges that incident nodes outside of \mathbf{s}^t are carried from \mathbf{A}^t to \mathbf{A}^{t-1} . Such formulation significantly boosts generation speed.

3.3. Learning the reverse process

We optimize the model parameters θ by maximizing the variational lower bound (VLB) of $\log p(\mathbf{A}^0)$. Following Sohl-Dickstein et al. (2015); Ho et al. (2020), the VLB is:

$$\begin{aligned} \mathcal{L}(\mathbf{A}^0; \theta) &= \mathbb{E}_q \left[\log \frac{p_\theta(\mathbf{A}^{0:T}, \mathbf{s}^{1:T})}{q(\mathbf{A}^{1:T}, \mathbf{s}^{1:T} | \mathbf{A}^0)} \right] \\ &= \mathbb{E}_q \left[\log \frac{p(\mathbf{A}^T)}{q(\mathbf{A}^T | \mathbf{A}^0)} + \underbrace{\log p_\theta(\mathbf{A}^0 | \mathbf{A}^1, \mathbf{s}^1)}_{\text{reconstruction term } \mathcal{L}_{\text{rec}}} + \right. \\ &\quad \left. \sum_{t=2}^T \underbrace{\log \frac{p_\theta(\mathbf{A}^{t-1} | \mathbf{A}^t, \mathbf{s}^t)}{q(\mathbf{A}^{t-1} | \mathbf{A}^t, \mathbf{s}^t, \mathbf{A}^0)}}_{\text{edge prediction term } \mathcal{L}_{\text{edge}}(t)} + \sum_{t=1}^T \underbrace{\log \frac{p_\theta(\mathbf{s}^t | \mathbf{A}^t)}{q(\mathbf{s}^t | \mathbf{A}^t, \mathbf{A}^0)}}_{\text{node selection term } \mathcal{L}_{\text{node}}(t)} \right]. \end{aligned} \quad (7)$$

(See Appendix B.1 for detailed derivation.) The first term contains no learnable parameters. The second term measures the reconstruction likelihood. For the edge prediction term $\mathcal{L}_{\text{edge}}(t)$, unlike Sohl-Dickstein et al. (2015); Ho et al. (2020), the posterior $q(\mathbf{A}^{t-1} | \mathbf{A}^t, \mathbf{s}^t, \mathbf{A}^0)$ is hard to compute, forbidding one to optimize $\mathcal{L}_{\text{edge}}(t)$ in a Rao-Blackwellized way. Since the entropy $\mathbb{H}[q(\mathbf{A}^{t-1} | \mathbf{A}^t, \mathbf{s}^t, \mathbf{A}^0)]$ is a constant, we consider optimizing the cross entropy in $\mathcal{L}_{\text{edge}}(t)$ via Monte Carlo estimates. We leave the work of variance reduction to the future.

For the node selection term $\mathcal{L}_{\text{node}}(t)$, we show that $q(\mathbf{s}^t | \mathbf{A}^t, \mathbf{A}^0)$ has closed-form expression. In particular, we first derive the posterior of the node degree distribution

$q(\mathbf{d}^t | \mathbf{A}^t, \mathbf{A}^0)$, whose form is as follows:

$$q(\mathbf{d}^{t-1} | \mathbf{A}^t, \mathbf{A}^0) = q(\mathbf{d}^{t-1} | \mathbf{d}^t, \mathbf{d}^0) = \prod_{i=1}^N q(\mathbf{d}_i^{t-1} | \mathbf{d}_i^t, \mathbf{d}_i^0),$$

where $q(\mathbf{d}_i^{t-1} | \mathbf{d}_i^t, \mathbf{d}_i^0) = \text{Bin}(k = \Delta_i^t, n = \Delta_i^0, p = \gamma_t)$, with $\Delta_i^t = \mathbf{d}_i^{t-1} - \mathbf{d}_i^t$, $\Delta_i^0 = \mathbf{d}_i^0 - \mathbf{d}_i^t$, $\gamma_t = \frac{\beta_t \bar{\alpha}_{t-1}}{1 - \bar{\alpha}_t}$. (8)

Here $\text{bin}(k; n, p)$ is a binomial distribution parameterized by n and p . Intuitively, a node degree \mathbf{d}_i^{t-1} is only relevant to the node's degrees \mathbf{d}_i^0 and \mathbf{d}_i^t at steps 0 and t . The connections do not affect the degree probability since each edge is added or removed independently. We provide formal proof and discuss the forward node degree distribution in Appendix A.2.

Since $\mathbf{s}_i^t = \mathbf{1}[\mathbf{d}_i^{t-1} \neq \mathbf{d}_i^t]$, we can compute the probability $q(\mathbf{s}_i^t = 1 | \mathbf{d}_i^t, \mathbf{d}_i^0)$, which is $1 - q(\mathbf{d}_i^{t-1} = \mathbf{d}_i^t | \mathbf{d}_i^t, \mathbf{d}_i^0)$. Finally, we obtain the closed-form posterior:

$$\begin{aligned} q(\mathbf{s}^t | \mathbf{d}^t, \mathbf{d}^0) &= \prod_{i=1}^N q(\mathbf{s}_i^t | \mathbf{d}_i^t, \mathbf{d}_i^0), \text{ where} \\ q(\mathbf{s}_i^t | \mathbf{d}_i^t, \mathbf{d}_i^0) &= \mathcal{B}(\mathbf{s}_i^t; 1 - (1 - \gamma_t)^{\Delta_i^0}). \end{aligned} \quad (9)$$

The KL divergence $\mathcal{L}_{\text{node}}(t)$ turns out to be the comparisons between Bernoulli distributions.

3.4. Degree-guided graph generation

A notable property of our proposed generative process is that it allows the generation of graphs with prescribed node degrees. The degree sequence of a graph is often strongly correlated to its other statistics; we show how such a generation scheme can be naturally extended from the proposed framework.

We explicitly model node degrees \mathbf{d}^0 of a graph \mathbf{A}^0 as a random variable, then the forward process becomes

$$q(\mathbf{A}^{1:T} | \mathbf{A}^0) = q(\mathbf{A}^{1:T} | \mathbf{A}^0)q(\mathbf{d}^0 | \mathbf{A}^0). \quad (10)$$

We also include \mathbf{d}^0 into the generative model $p(\mathbf{A}^0, \mathbf{d}^0)$. If the model guarantees that \mathbf{d}^0 is the node degrees of \mathbf{A}^0 , then $p_\theta(\mathbf{A}^0) = p_\theta(\mathbf{A}^0, \mathbf{d}^0)$ still models graph data \mathbf{A}^0 . Even if $p_\theta(\mathbf{A}^0, \mathbf{d}^0)$ allows \mathbf{d}^0 to differ a little from the true node degrees, it is still valid to maximize the likelihood $p_\theta(\mathbf{A}^0, \mathbf{d}^0 = \mathbf{A}^0)$ because model training will encourage the model to generate \mathbf{A}^0 and \mathbf{d}^0 to match each other. We decompose the model by:

$$p_\theta(\mathbf{A}^0, \mathbf{d}^0) = p_\theta(\mathbf{d}^0)p_\theta(\mathbf{A}^0 | \mathbf{d}^0). \quad (11)$$

With this decomposition, we first sample arbitrary node degrees \mathbf{d}^0 from $p_\theta(\mathbf{d}^0)$, then generate a graph with the degree constraint (See Alg. 1). Correspondingly, the denoising model becomes

$$p_\theta(\mathbf{A}^{0:T}, \mathbf{s}^{1:T}, \mathbf{d}^0) = p_\theta(\mathbf{d}^0)p_\theta(\mathbf{A}^{0:T}, \mathbf{s}^{1:T} | \mathbf{d}^0). \quad (12)$$

We separate the optimizations for the node degree model $p_\theta(\mathbf{d}^0)$ and the graph denoising model $p_\theta(\mathbf{A}^{0:T}, \mathbf{s}^{1:T} | \mathbf{d}^0)$. The entire training objective is

$$\mathcal{L}(\mathbf{A}^0, \mathbf{d}^0; \theta) = \mathbb{E}_q \left[\underbrace{\log p_\theta(\mathbf{d}^0)}_{\mathcal{L}(\mathbf{d}^0; \theta)} + \underbrace{\log \frac{p_\theta(\mathbf{A}^{0:T}, \mathbf{s}^{1:T} | \mathbf{d}^0)}{q(\mathbf{A}^{0:T}, \mathbf{s}^{1:T} | \mathbf{A}^0)}}_{\mathcal{L}(\mathbf{A}^0 | \mathbf{d}^0; \theta)} \right].$$

(See Appendix B.2 for detailed derivation.) For $\mathcal{L}(\mathbf{d}^0; \theta)$, we treat the learning of node degree distribution as a sequence modeling task. The decomposition of $\mathcal{L}(\mathbf{A}^0 | \mathbf{d}^0; \theta)$ remains the same as Eqn. (7), except that all terms related to the graph denoising model are now conditioning on \mathbf{d}^0 . In particular, for the node selection distribution, we consider a special parameterization by setting $p_\theta(\mathbf{s}^t | \mathbf{A}^t, \mathbf{d}^0) := q(\mathbf{s}^t | \mathbf{d}^t, \mathbf{d}^0)$ in Eqn. (9). Note that now the node selection distribution contains no learnable parameters. Moreover, since the KL divergence $\mathcal{L}_{\text{node}}(t)$ is now zero, we can further simplify the $\mathcal{L}(\mathbf{A}^0 | \mathbf{d}^0; \theta)$ into

$$\mathcal{L}(\mathbf{A}^0 | \mathbf{d}^0; \theta) = \mathbb{E}_q \left[\log \frac{p(\mathbf{A}^T)}{q(\mathbf{A}^T | \mathbf{A}^0)} + \log p_\theta(\mathbf{A}^0 | \mathbf{A}^1, \mathbf{s}^1, \mathbf{d}^0) + \sum_{t=2}^T \log \frac{p_\theta(\mathbf{A}^{t-1} | \mathbf{A}^t, \mathbf{s}^t, \mathbf{d}^0)}{q(\mathbf{A}^{t-1} | \mathbf{A}^t, \mathbf{s}^t, \mathbf{A}^0)} \right]. \quad (13)$$

In our framework, the node degree constraint \mathbf{d}^0 is mainly imposed on $p_\theta(\mathbf{s}^t | \mathbf{A}^t, \mathbf{d}^0)$ – only nodes with a degree below the specified degree \mathbf{d}^0 may be selected to participate in the edge prediction. On the other hand, though the exact probability $p_\theta(\mathbf{A}^{t-1} | \mathbf{A}^t, \mathbf{s}^t, \mathbf{d}^0)$ includes information about the maximum number of edges ($\mathbf{d}^0 - \mathbf{d}^t$) that can be added to nodes, this can be not easy to track during the edge formation. Here we consider simply augmenting the inputs to the neural network with \mathbf{d}^0 . In practice, we found that the specified node degrees \mathbf{d}^0 can accurately control the actual node degrees of the generated graphs.

Algorithm 1 Degree-guided graph generation

Input: Empty graph \mathbf{A}^T , graph model $p_\theta(\mathbf{A}^{t-1} | \mathbf{A}^t, \mathbf{s}^t)$, degree sequence model $p_\theta(\mathbf{d}^0)$, and diffusion steps T .
Output: Generated graph \mathbf{A}^0
 Draw $\mathbf{d}^0 \sim p_\theta(\mathbf{d}^0)$
for $t = T, \dots, 1$ **do**
 Draw $\mathbf{s}^t \sim q(\mathbf{s}^t | \deg(\mathbf{A}^t), \mathbf{d}^0)$.
 Draw $\mathbf{A}^{t-1} \sim p_\theta(\mathbf{A}^{t-1} | \mathbf{A}^t, \mathbf{s}^t)$.
end for

Degree-guided generation turns out to be very expressive in modeling large graphs. We reason that the \mathbf{d}^0 significantly reduces the possible trajectories a graph can evolve along, thus reducing the modeling complexity.

3.5. Implementation

We briefly describe the implementation of $p_\theta(\mathbf{s}^t | \mathbf{A}^t)$, $p_\theta(\mathbf{A}^{t-1} | \mathbf{A}^t, \mathbf{s}^t)$, and $p_\theta(\mathbf{d}^0)$. Note we use the same architecture for $p_\theta(\mathbf{A}^{t-1} | \mathbf{A}^t, \mathbf{s}^t)$ and $p_\theta(\mathbf{A}^{t-1} | \mathbf{A}^t, \mathbf{s}^t, \mathbf{d}^0)$, except the inputs of the latter are augmented with \mathbf{d}^0 . We treat $p_\theta(\mathbf{s}^t | \mathbf{A}^t)$ as a node classification problem. We implement it with an MPNN, which takes \mathbf{A}^t as the input and computes node representations $\mathbf{Z}^t \in \mathbb{R}^{N \times d_h}$ for all nodes. The hidden dimension d_h is a hyper-parameter here. The edge prediction model $p_\theta(\mathbf{A}^{t-1} | \mathbf{A}^t, \mathbf{s}^t)$ is a link prediction model. It shares the MPNN and uses node representations $\mathbf{Z}^t[\mathbf{s}^t]$ to predict links between nodes indicated by \mathbf{s}^t . For the node degree model $p_\theta(\mathbf{d}^0)$, if there are multiple graphs in the dataset, we use a recurrent neural network (RNN) to fit the histogram of node degrees. If there is only one graph with node degrees \mathbf{d}^0 , the probability mass of the event \mathbf{d}^0 is directly set to 1. Detailed implementations are in Appendix C.

3.6. Model analysis

Complexity analysis. Let integer M represent the number of edges in a graph, and K be the maximum number of active nodes during the reverse process. In each generation step t , the MPNN needs $O(M)$ operations to compute node representations, $O(N)$ operations to predict \mathbf{s}^t , and $O(K^2)$ operations to predict links between K active nodes. The factor K is relevant to the noise scheduling. We find that K is smaller than N by at least one order of magnitude when we use linear noise scheduling. In a total of T generation steps, the overall running time $O(T \max(K^2, M))$. As a comparison, previous diffusion-based models need running time $O(TN^2)$ because they need to make $O(N^2)$ link predictions at each time step.

Expressivity analysis. EDGE modifies a graph for multiple iterations to generate a sample. In each iteration, new

edges are added to the graph according to the graph structure of the prior iteration. Therefore, EDGE is NOT constrained by the limitation of edge independence and thus has a fundamental advantage over edge-independent models.

The ability of EDGE might be affected by the underlying MPNN, e.g., the neural network may learn the same node representations from different subgraph structures (Xu et al., 2018). However, this issue can be overcome by choosing more expressive GNNs (Sato, 2020). We defer such discussion to future work.

4. Related Works

Edge-independent models, which assume edges are formed independently with some probabilities, are prevalent in modeling large networks. This model category includes classical models such as ER graph model (Erdos et al., 1960), SBM (Holland et al., 1983), and recent deep models such as variational graph auto-encoders (Kipf & Welling, 2016b; Mehta et al., 2019; Li et al., 2020; Chen et al., 2022a), NetGAN and its variant (Bojchevski et al., 2018; Rendsburg et al., 2020). Recent works pointed out that these models can not reproduce desiring statistics of the target network, such as triangle counts, clustering coefficient, and square counts (Seshadhri et al., 2020; Chanpuriya et al., 2021).

Deep auto-regressive (AR) graph models (Li et al., 2018; You et al., 2018; Liao et al., 2019; Zang & Wang, 2020; Chen et al., 2021; Han et al., 2023) generate graph edges by sequentially filling up an adjacency matrix to generate a graph. These algorithms are slow because they need to make N^2 predictions. Dai et al. (2020) proposes a method to leverage graph sparsity and predict only non-zero entries in the adjacency matrix. The sequential structure also poses limitations to their modeling abilities. Long-term memory is a typical issue of these sequential models, so it is hard for them to model global graph properties. Moreover, the performance of such models depends on the node orderings of the training data.

Diffusion-based generative models are shown to be powerful in generating high-quality graphs (Niu et al., 2020; Liu et al., 2019; Jo et al., 2022; Haefeli et al., 2022; Chen et al., 2022b; Vignac et al., 2022; Kong et al.). By “tailoring” a graph with multiple steps, these models can model edge correlations. They do not have the two limitations of auto-regressive modes either. However, all previous diffusion-based models focus on generation tasks with small graphs. This work identifies and addresses two obstacles that forbid diffusion-based models from modeling large graphs.

5. Experiments

We empirically verify the effectiveness of our proposed approach from the perspectives of capturing training distri-

	#nodes	#edges	#graphs	feature
Community	[60, 160]	[231, 1,965]	510	
Ego	[50, 399]	[57, 1,071]	757	
QM9	[1,9]	[0, 28]	133,885	✓
Polblogs	1,222	16,714	1	
Cora	2,485	5,069	1	
Road-MN	2,640	6,604	1	
PPI	3,852	37,841	1	

Table 1. Dataset statistics

bution and generation efficiency ¹.

5.1. Experimental setup

Datasets. We conduct experiments on both generic graph datasets and large networks. The generic graph datasets consist of multiple graphs of varying sizes. Here we consider Community and Ego datasets (You et al., 2018), all of which contain graphs with hundreds of nodes. We consider three networks, Polblogs (Adamic & Glance, 2005), Cora (Sen et al., 2008), Road-Minnesota (Rossi & Ahmed, 2015) and PPI (Stark et al., 2010). Each of these networks contains thousands of nodes. We also use the QM9 dataset (Ramakrishnan et al., 2014) to demonstrate that EDGE can be easily extended to generate featured graphs. The statistics of the datasets are shown in Table 1.

Baselines. For generic graphs, We compare EDGE to six recent deep generative graph models, which include two auto-regressive graph models, GraphRNN (You et al., 2018) and GRAN (Liao et al., 2019), three diffusion-based models, GDSS (Jo et al., 2022), DiscDDPM (Haefeli et al., 2022) and DiGress (Vignac et al., 2022), and one flow-based model, GraphCNF (Lippe & Gavves, 2020). For large networks, we follow Chanpuriya et al. (2021) and use six edge-independent models, which include VGAE (Kipf & Welling, 2016b), CELL (Rendsburg et al., 2020), TSVD (Seshadhri et al., 2020), and three methods proposed by Chanpuriya et al. (2021) (CCOP, HDOP, Linear). We also include GraphRNN as a baseline because it is still affordable to train it on large networks. For the QM9 dataset, We compare EDGE against GDSS (Jo et al., 2022) and DiGress (Vignac et al., 2022).

Evaluation. We examine the generated generic graphs with both structure-based and neural-based metrics. For structure-based metrics, we evaluate the Maximum Mean Discrepancy (MMD) (Gretton et al., 2012) between the test graphs and the generated graphs in terms of degrees, clustering coefficients, and orbit counts (You et al., 2018). For neural-based metrics, we evaluate the FID and the MMD RBF metrics proposed by Thompson et al. (2022). All im-

¹Code is available at github.com/tufts-ml/graph-generation-EDGE

	Community					Ego				
	Structure-based (MMD)		Orb.	Neural-based		Structure-based (MMD)		Orb.	Neural-based	
	Deg.	Clus.		FID	RBF MMD	Deg.	Clus.		FID	RBF MMD
GRNN	0.1440	<u>0.0535</u>	0.0198	8.3869	0.1591	<u>0.0768</u>	1.1456	0.1087	90.5655	0.6827
GRAN	0.1022	0.0894	0.0198	64.1145	0.0749	0.5778	<u>0.3360</u>	0.0406	489.9598	0.2633
GraphCNF	0.1129	1.2882	0.0197	29.1526	0.1341	0.1010	0.7654	0.0820	18.7929	0.0896
GDSS	0.0535	0.2072	0.0196	6.5531	<u>0.0443</u>	0.8189	0.6032	0.3315	60.6100	0.4331
DiscDDPM	0.1238	0.6549	<u>0.0246</u>	8.6321	0.0840	0.4613	<u>0.1681</u>	<u>0.0633</u>	42.7994	0.1561
DiGress	0.0409	0.0167	0.0298	3.4261	0.0460	0.0708	0.0092	0.1205	18.6794	0.0489
EDGE	0.0175	0.0689	0.0198	2.2378	0.0227	0.0579	0.1773	0.0519	15.7614	0.0658

Table 2. Generation performance on generic graphs. We used unpaired t-tests to compare the results; the numbers in bold indicate the method is better at the 5% significance level, and the second-best method is underlined. We provide standard deviation in Appendix F.

plementations of the evaluation are provided by Thompson et al. (2022). For all these metrics, the smaller, the better.

For each large network, we follow Chanpuriya et al. (2021) and evaluate how well the graph statistics of the generated network can match ground truths, which are statistics computed from training data. We consider the following statistics: power-law exponent of the degree sequence (PLE); normalized triangle counts (NTC); global clustering coefficient (CC) (Chanpuriya et al., 2021); characteristic path length (CPL); and assortativity coefficient (AC) (Newman, 2002). We also report the edge overlap ratio (EO) between the generated network and the original one to check whether a model performs well by simply memorizing the data. A good model should generate graphs with statistics similar to the ground truths. At the same time, the edge overlap should be small, indicating that the model does not simply memorize the data.

For the QM9 dataset, we evaluate the Validity, Uniqueness, Fréchet ChemNet Distance (Preuer et al., 2018) and Scaffold similarity (Bemis & Murcko, 1996) on the samples generated from baselines and our proposed method. We use molsets library (Polykovskiy et al., 2020) to implement the evaluation.

5.2. Evaluation of sample quality

Generic graph generation. Table 2 summarizes the evaluation of generated graphs on the Community and Ego datasets. EDGE achieve competitive performance on both datasets, outperforming all baselines on 8 out of 10 metrics. Our method scores second for the other two metrics and is slightly worse than the best. We hypothesize that the degree sequence of a graph is highly correlated to the graph structure. Since the node degrees explicitly guide the generation of a graph, other graph statistics are also improved.

Large network generation. Unlike edge-independent models, the edge overlap ratios in the GraphRNN and our approach are not tunable. To make a fair comparison, we

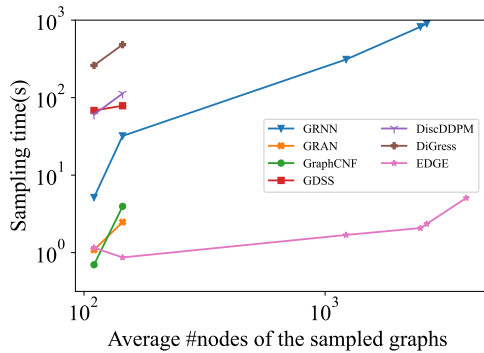


Figure 3. Sampling speed comparison over different models.

report the performance of the edge-independent models that have similar or higher EO than the deep generative approaches. Table 3 shows the statistics of the network itself (labeled as “True”) and statistics computed from generated graphs. Our approach shows superior performance on all three networks. The performance improvement on the Cora dataset is less obvious. We believe this is because the graph is highly sparse – the message-passing neural model may not work at full strength. We notice that GraphRNN can not even compete with edge-independent models. We also visualize the generated graphs of Polblogs in Figure 4.

5.3. Efficiency

We compare the sampling efficiency of EDGE against other deep generative graph models. We estimate the average time for a model to sample one graph to make a consistent comparison over all datasets. The average sampling time for each dataset is averaged over 128 runs. Figure 3 shows the relationship between the sampling speed and the graph size. Except for GraphRNN, all baselines can only generate graphs for Community and Ego datasets, which contain 110 and 144 nodes on average. Our approach runs only slower than GraphCNF on the Community dataset by 0.5s. On large graphs, our model has a clear advantage in terms of running time. Note that our model spends less time on an Ego graph than a Community graph, though an Ego graph, on average, contains more nodes than a Community graph.

Polblogs						Cora						
	EO	PLE	NTC	CC	CPL	AC	EO	PLE	NTC	CC	CPL	AC
True	100	1.414	1	0.226	2.738	-0.221	100	1.885	1	0.090	6.311	-0.071
OPB	24.5	1.395	0.667	0.150	2.524	-0.143	10.9	1.852	0.097	0.008	4.476	-0.037
HDOP	16.4	1.393	0.687	0.153	2.522	-0.131	0.9	1.849	0.113	0.009	4.770	-0.030
CELL	26.8	1.385	0.810	0.211	2.534	-0.230	10.3	1.774	0.009	0.002	5.799	-0.018
CO	20.1	1.975	0.045	0.028	2.502	0.068	9.7	1.776	0.009	0.002	5.653	0.010
TSVD	32.0	1.373	0.872	0.205	2.532	-0.216	6.7	1.858	0.349	0.028	4.908	-0.006
VGAE	3.6	1.723	0.05	0.001	2.531	-0.086	1.5	1.717	0.120	0.220	4.934	0.002
GRNN	9.6	1.333	0.354	0.095	2.566	0.096	0.4	1.822	0.043	0.011	6.146	0.043
EDGE	16.5	1.398	0.977	0.217	2.647	-0.214	1.1	1.755	0.446	0.034	4.995	-0.046
Road-Minnesota						PPI						
	EO	PLE	NTC	CC	CPL	AC	EO	PLE	NTC	CC	CPL	AC
True	100	2.147	1	0.028	35.349	-0.187	100	1.462	1	0.092	3.095	-0.099
OPB	29.7	2.188	0.083	0.002	8.036	0.009	16.3	1.443	0.640	0.058	2.914	-0.089
HDOP	13.2	2.192	0.208	0.004	8.274	-0.024	6.9	1.444	0.638	0.058	2.917	-0.086
CELL	30.7	2.267	0.053	0.001	10.219	-0.082	6.7	1.400	0.248	0.040	3.108	0.176
CO	19.8	2.044	2.845	0.040	11.478	-0.012	9.9	1.754	0.015	0.006	3.046	0.043
TSVD	19.4	2.172	0.060	0.001	8.431	0.006	13.2	1.426	0.848	0.077	2.867	-0.089
VGAE	1.3	1.678	0.096	0.009	11.120	-0.027	0.5	1.362	0.091	0.012	2.991	0.054
GRNN	0.6	1.570	0.099	0.007	11.695	0.006	OOD	OOD	OOD	OOD	OOD	OOD
EDGE	0.8	1.910	0.962	0.011	9.125	-0.063	7.5	1.449	0.981	0.091	3.028	-0.107

Table 3. Graph statistics of generated large networks. EDGE generates graphs with statistics that are much closer to the ground truths.

	Validity↑	Uniqueness↑	FCD↓	Scaf. Sim.↑
GDSS	95.7	98.5	2.9	-
DiGress	99.0	100	0.151	0.908
EDGE	99.1	100	0.458	0.763

Table 4. Generative performance on the QM9 dataset

This is because the computation of our model scales with the number of edges, and Ego graphs are often sparser than Community graphs.

5.4. Generative performance on QM9 dataset

We further investigate the potential of extending EDGE towards generative feature graphs. To do this, we develop a hierarchical generation process that incorporates EDGE as an intermediate component of the hierarchical framework. More details on this development can be found in Appendix E. Our effectiveness analysis of the model is based on the QM9 dataset, and our results demonstrate that the extended EDGE model is competitive with GDSS and DiGress, as shown in Table 4.

5.5. Ablation studies

Diffusion variants. We show that the random variables $s^{1:T}$ and d^0 play important roles in EDGE’s good performances. Table 5 shows the generative performance on the

	$s^{1:T}$	d^0	PLE	NTC	CC	CPL	AC	Speed
True			1.414	1	0.226	2.738	-0.221	
G(N,0.5)			OOD	OOD	OOD	OOD	OOD	
G(N,0)			1.341	3.234	0.237	2.747	-0.304	15.3s
G(N,0)	✓		1.383	2.364	0.251	2.638	-0.331	2.1s
G(N,0)	✓	✓	1.398	0.977	0.217	2.647	-0.214	1.7s

Table 5. Performance of EDGE’s variants on the Polblogs dataset.

Polblogs dataset for four diffusion configurations. There are no innovations in the first two configurations: we use the basic model introduced in Section 2 and the same denoising network used in EDGE. However, this network needs to predict edges between all node pairs. If we set the convergent distribution to $G(N, 0.5)$, we can not even train such a model due to the limit of GPU memory. This justifies our use of $G(N, 0)$ as the convergent distribution. The introduction of $s^{1:T}$ (Section 3.2) significantly improves the sampling speed. Finally, the EDGE approach, which explicitly models node degrees d^0 and generates graphs with degree guidance, excels over all the other variants regarding both generative performance and sampling speed.

Diffusion steps vs. model performance. In EDGE, the number of diffusion steps T decides how many nodes would actively participate in the edge prediction. Here we investigate how it affects the model performance under linear noise scheduling.

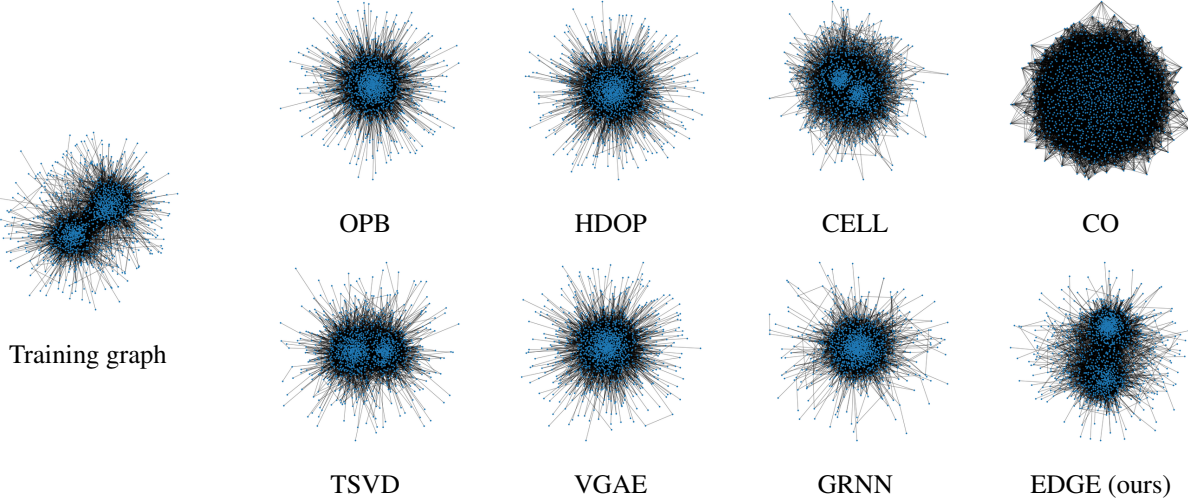


Figure 4. Visualization of samples for the Polblogs dataset. We observe that only CELL, TSVD, and EDGE can learn the basic structure of the ground-truth network, while other baselines fail. The network sampled from EDGE appears to be more similar to the training graph.

	EO	PLE	NTC	CC	CPL	AC
Polblogs	True	100	1.414	1	0.226	2.738
	64	1.8	1.380	1.148	0.235	2.800
	128*	14.9	1.386	1.030	0.238	2.747
	256*	16.5	1.398	0.977	0.217	2.647
	512*	15.0	1.398	0.923	0.218	2.635
	1024*	16.5	1.400	0.991	0.219	2.665
Cora	True	100	1.885	1	0.090	6.311
	64*	0.9	1.755	0.446	0.034	4.995
	128	1.1	1.747	0.555	0.042	5.017
	256	0.8	1.753	0.360	0.027	4.818
	512	0.8	1.753	0.360	0.027	4.818
	1024	0.9	1.762	0.348	0.027	4.778
Road-MN	True	100	2.147	1	0.028	35.349
	64*	0.8	1.910	0.962	0.011	9.125
	128	1.2	1.803	1.232	0.041	6.501
	256	0.8	1.953	1.057	0.014	7.471
	512	1.3	1.965	1.472	0.020	7.710
	1024	1.2	1.983	2.491	0.035	7.906
PPI	True	100	1.462	1	0.092	3.095
	64	7.4	1.421	2.455	-0.116	3.498
	128	6.2	1.419	1.503	0.126	3.384
	256*	7.5	1.449	0.981	0.091	3.028
	512*	7.0	1.438	1.101	0.099	3.244
	1024*	7.1	1.441	0.925	0.074	3.150

Table 6. Large diffusion steps T does not necessarily improve model performance. Good diffusion steps are labeled with “*”.

Specifically, we train our model on three large networks with $T \in \{64, 128, 256, 512, 1024\}$ and report the model performance in Table 6. Surprisingly, unlike traditional diffusion models in which more diffusion steps usually yield better performance, the effect of T on our model performance requires further analyses. For instance, $T = 64$

gives the best performance in the Cora and Road-Minnesota datasets. This is likely because they are very sparse, and fewer active nodes and edges can be predicted for each step using a large diffusion step T . The lack of training signals may lead to poor model convergence. Such an issue is not observed for relatively denser graphs, e.g., Polblogs and PPI datasets. Moreover, for these two datasets, it is necessary to use a large T to guarantee the model performance. When T is large enough ($T = 128$ for Polblogs and $T = 256$ for PPI), further increasing T does not improve the model performance.

6. Conclusion

In this work, we propose EDGE, a generative graph model based on a discrete diffusion process. By leveraging the sparsity in the diffusion process, EDGE significantly improves the computation efficiency and scales to graphs with thousands of nodes. By explicitly modeling node degrees, EDGE gains the advantage of capturing important graph statistics in training distributions. The empirical study shows EDGE’s superior performance in several graph generation tasks.

References

- Adamic, L. A. and Glance, N. The political blogosphere and the 2004 us election: divided they blog. In *Proceedings of the 3rd international workshop on Link discovery*, pp. 36–43, 2005.
- Austin, J., Johnson, D. D., Ho, J., Tarlow, D., and van den Berg, R. Structured denoising diffusion models in discrete state-spaces. *Advances in Neural Information Processing Systems*, 34:17981–17993, 2021.

- Bemis, G. W. and Murcko, M. A. The properties of known drugs. 1. molecular frameworks. *Journal of medicinal chemistry*, 39(15):2887–2893, 1996.
- Bojchevski, A., Shchur, O., Zügner, D., and Günnemann, S. Netgan: Generating graphs via random walks. In *International conference on machine learning*, pp. 610–619. PMLR, 2018.
- Broido, A. D. and Clauset, A. Scale-free networks are rare. *Nature communications*, 10(1):1–10, 2019.
- Chakrabarti, D. and Faloutsos, C. Graph mining: Laws, generators, and algorithms. *ACM computing surveys (CSUR)*, 38(1):2–es, 2006.
- Chanpuriya, S., Musco, C., Sotiroopoulos, K., and Tsourakakis, C. On the power of edge independent graph models. *Advances in Neural Information Processing Systems*, 34:24418–24429, 2021.
- Chen, X., Han, X., Hu, J., Ruiz, F. J., and Liu, L. Order matters: Probabilistic modeling of node sequence for graph generation. *arXiv preprint arXiv:2106.06189*, 2021.
- Chen, X., Chen, X., and Liu, L. Interpretable node representation with attribute decoding. *arXiv preprint arXiv:2212.01682*, 2022a.
- Chen, X., Li, Y., Zhang, A., and Liu, L.-p. Nvdiff: Graph generation through the diffusion of node vectors. *arXiv preprint arXiv:2211.10794*, 2022b.
- Cho, K., Van Merriënboer, B., Bahdanau, D., and Bengio, Y. On the properties of neural machine translation: Encoder–decoder approaches. *arXiv preprint arXiv:1409.1259*, 2014.
- Dai, H., Nazi, A., Li, Y., Dai, B., and Schuurmans, D. Scalable deep generative modeling for sparse graphs. In *International conference on machine learning*, pp. 2302–2312. PMLR, 2020.
- Devlin, J., Chang, M.-W., Lee, K., and Toutanova, K. Bert: Pre-training of deep bidirectional transformers for language understanding. *arXiv preprint arXiv:1810.04805*, 2018.
- Dhariwal, P. and Nichol, A. Diffusion models beat gans on image synthesis. *Advances in Neural Information Processing Systems*, 34:8780–8794, 2021.
- Du, Y., Wang, S., Guo, X., Cao, H., Hu, S., Jiang, J., Varala, A., Angirekula, A., and Zhao, L. Graphgt: Machine learning datasets for graph generation and transformation. In *Thirty-fifth Conference on Neural Information Processing Systems Datasets and Benchmarks Track (Round 2)*, 2021.
- Elfwing, S., Uchibe, E., and Doya, K. Sigmoid-weighted linear units for neural network function approximation in reinforcement learning. *Neural Networks*, 107:3–11, 2018.
- Erdos, P., Rényi, A., et al. On the evolution of random graphs. *Publ. Math. Inst. Hung. Acad. Sci.*, 5(1):17–60, 1960.
- Fey, M. and Lenssen, J. E. Fast graph representation learning with pytorch geometric. *arXiv preprint arXiv:1903.02428*, 2019.
- Gretton, A., Borgwardt, K. M., Rasch, M. J., Schölkopf, B., and Smola, A. A kernel two-sample test. *The Journal of Machine Learning Research*, 13(1):723–773, 2012.
- Haefeli, K. K., Martinkus, K., Perraudeau, N., and Wattehhofer, R. Diffusion models for graphs benefit from discrete state spaces. *arXiv preprint arXiv:2210.01549*, 2022.
- Han, X., Chen, X., Ruiz, F. J., and Liu, L.-P. Fitting autoregressive graph generative models through maximum likelihood estimation. *Journal of Machine Learning Research*, 24(97):1–30, 2023.
- Ho, J., Jain, A., and Abbeel, P. Denoising diffusion probabilistic models. *Advances in Neural Information Processing Systems*, 33:6840–6851, 2020.
- Holland, P. W., Laskey, K. B., and Leinhardt, S. Stochastic blockmodels: First steps. *Social networks*, 5(2):109–137, 1983.
- Hoogeboom, E., Nielsen, D., Jaini, P., Forré, P., and Welling, M. Argmax flows and multinomial diffusion: Learning categorical distributions. *Advances in Neural Information Processing Systems*, 34:12454–12465, 2021.
- Jo, J., Lee, S., and Hwang, S. J. Score-based generative modeling of graphs via the system of stochastic differential equations. *arXiv preprint arXiv:2202.02514*, 2022.
- Kingma, D. P. and Ba, J. Adam: A method for stochastic optimization. *arXiv preprint arXiv:1412.6980*, 2014.
- Kipf, T. N. and Welling, M. Semi-supervised classification with graph convolutional networks. *arXiv preprint arXiv:1609.02907*, 2016a.
- Kipf, T. N. and Welling, M. Variational graph auto-encoders. *arXiv preprint arXiv:1611.07308*, 2016b.
- Kong, L., Cui, J., Sun, H., Zhuang, Y., Prakash, B. A., and Zhang, C. Autoregressive diffusion model for graph generation.

- Li, J., Yu, J., Li, J., Zhang, H., Zhao, K., Rong, Y., Cheng, H., and Huang, J. Dirichlet graph variational autoencoder. *Advances in Neural Information Processing Systems*, 33: 5274–5283, 2020.
- Li, Y., Vinyals, O., Dyer, C., Pascanu, R., and Battaglia, P. Learning deep generative models of graphs. *arXiv preprint arXiv:1803.03324*, 2018.
- Liao, R., Li, Y., Song, Y., Wang, S., Hamilton, W., Duvenaud, D. K., Urtasun, R., and Zemel, R. Efficient graph generation with graph recurrent attention networks. In *Advances in Neural Information Processing Systems*, pp. 4255–4265, 2019.
- Lippe, P. and Gavves, E. Categorical normalizing flows via continuous transformations. *arXiv preprint arXiv:2006.09790*, 2020.
- Liu, J., Kumar, A., Ba, J., Kiros, J., and Swersky, K. Graph normalizing flows. *Advances in Neural Information Processing Systems*, 32, 2019.
- Lusher, D., Koskinen, J., and Robins, G. *Exponential random graph models for social networks: Theory, methods, and applications*. Cambridge University Press, 2013.
- Madhawa, K., Ishiguro, K., Nakago, K., and Abe, M. Graph-nvp: An invertible flow model for generating molecular graphs. *arXiv preprint arXiv:1905.11600*, 2019.
- Mehta, N., Duke, L. C., and Rai, P. Stochastic blockmodels meet graph neural networks. In *International Conference on Machine Learning*, pp. 4466–4474. PMLR, 2019.
- Newman, M. E. Assortative mixing in networks. *Physical review letters*, 89(20):208701, 2002.
- Newman, M. E., Watts, D. J., and Strogatz, S. H. Random graph models of social networks. *Proceedings of the national academy of sciences*, 99(suppl_1):2566–2572, 2002.
- Niu, C., Song, Y., Song, J., Zhao, S., Grover, A., and Ermon, S. Permutation invariant graph generation via score-based generative modeling. In *International Conference on Artificial Intelligence and Statistics*, pp. 4474–4484. PMLR, 2020.
- O’Bray, L., Horn, M., Rieck, B., and Borgwardt, K. Evaluation metrics for graph generative models: Problems, pitfalls, and practical solutions. *arXiv preprint arXiv:2106.01098*, 2021.
- Paszke, A., Gross, S., Massa, F., Lerer, A., Bradbury, J., Chanan, G., Killeen, T., Lin, Z., Gimelshein, N., Antiga, L., et al. Pytorch: An imperative style, high-performance deep learning library. *Advances in neural information processing systems*, 32, 2019.
- Polykovskiy, D., Zhebrak, A., Sanchez-Lengeling, B., Golovanov, S., Tatanov, O., Belyaev, S., Kurbanov, R., Artamonov, A., Aladinskiy, V., Veselov, M., et al. Molecular sets (moses): a benchmarking platform for molecular generation models. *Frontiers in pharmacology*, 11:565644, 2020.
- Preuer, K., Renz, P., Unterthiner, T., Hochreiter, S., and Klambauer, G. Fréchet chemnet distance: a metric for generative models for molecules in drug discovery. *Journal of chemical information and modeling*, 58(9):1736–1741, 2018.
- Ramakrishnan, R., Dral, P. O., Rupp, M., and Von Lilienfeld, O. A. Quantum chemistry structures and properties of 134 kilo molecules. *Scientific data*, 1(1):1–7, 2014.
- Rendsburg, L., Heidrich, H., and Von Luxburg, U. Netgan without gan: From random walks to low-rank approximations. In *International Conference on Machine Learning*, pp. 8073–8082. PMLR, 2020.
- Rossi, R. and Ahmed, N. The network data repository with interactive graph analytics and visualization. In *Proceedings of the AAAI conference on artificial intelligence*, volume 29, 2015.
- Sato, R. A survey on the expressive power of graph neural networks. *arXiv preprint arXiv:2003.04078*, 2020.
- Schuster, M. and Paliwal, K. K. Bidirectional recurrent neural networks. *IEEE transactions on Signal Processing*, 45(11):2673–2681, 1997.
- Sen, P., Namata, G., Bilgic, M., Getoor, L., Galligher, B., and Eliassi-Rad, T. Collective classification in network data. *AI magazine*, 29(3):93–93, 2008.
- Seshadhri, C., Sharma, A., Stolman, A., and Goel, A. The impossibility of low-rank representations for triangle-rich complex networks. *Proceedings of the National Academy of Sciences*, 117(11):5631–5637, 2020.
- Shi, Y., Huang, Z., Feng, S., Zhong, H., Wang, W., and Sun, Y. Masked label prediction: Unified message passing model for semi-supervised classification. *arXiv preprint arXiv:2009.03509*, 2020.
- Sohl-Dickstein, J., Weiss, E., Maheswaranathan, N., and Ganguli, S. Deep unsupervised learning using nonequilibrium thermodynamics. In *International Conference on Machine Learning*, pp. 2256–2265. PMLR, 2015.
- Stark, C., Breitkreutz, B.-J., Chatr-Aryamontri, A., Boucher, L., Oughtred, R., Livstone, M. S., Nixon, J., Van Auken, K., Wang, X., Shi, X., et al. The biogrid interaction database: 2011 update. *Nucleic acids research*, 39(suppl_1):D698–D704, 2010.

Thompson, R., Knyazev, B., Ghalebi, E., Kim, J., and Taylor, G. W. On evaluation metrics for graph generative models. *arXiv preprint arXiv:2201.09871*, 2022.

Vignac, C., Krawczuk, I., Siraudin, A., Wang, B., Cevher, V., and Frossard, P. Digress: Discrete denoising diffusion for graph generation. *arXiv preprint arXiv:2209.14734*, 2022.

Xu, K., Hu, W., Leskovec, J., and Jegelka, S. How powerful are graph neural networks? In *International Conference on Learning Representations*, 2018.

Ying, X. and Wu, X. Graph generation with prescribed feature constraints. In *Proceedings of the 2009 SIAM International Conference on Data Mining*, pp. 966–977. SIAM, 2009.

You, J., Ying, R., Ren, X., Hamilton, W. L., and Leskovec, J. GraphRNN: Generating realistic graphs with deep auto-regressive models. *arXiv preprint arXiv:1802.08773*, 2018.

Zang, C. and Wang, F. Moflow: an invertible flow model for generating molecular graphs. In *Proceedings of the 26th ACM SIGKDD International Conference on Knowledge Discovery & Data Mining*, pp. 617–626, 2020.

Appendix

A. Derivation of the $G(N, 0)$ Diffusion Process and the Degree Change Distribution

We first derive the forward and reverse transition distribution of the $G(N, 0)$ diffusion process, then, based on the derived results, we elaborate on the node degree change distributions for both directions.

A.1. The $G(N, 0)$ diffusion process

We consider modeling the upper triangle of the adjacency matrix \mathbf{A}^0 . Since we have $p = 0$ in our framework, for the forward transition kernel, we have

$$q(\mathbf{A}^t | \mathbf{A}^{t-1}) = \prod_{i,j: i < j} q(\mathbf{A}_{i,j}^t | \mathbf{A}_{i,j}^{t-1}), \text{ with } q(\mathbf{A}_{i,j}^t | \mathbf{A}_{i,j}^{t-1}) = \mathcal{B}(\mathbf{A}_{i,j}^t; (1 - \beta_t) \mathbf{A}_{i,j}^{t-1}). \quad (14)$$

$$q(\mathbf{A}^t | \mathbf{A}^0) = \prod_{i,j: i < j} q(\mathbf{A}_{i,j}^t | \mathbf{A}_{i,j}^0), \text{ with } q(\mathbf{A}_{i,j}^t | \mathbf{A}_{i,j}^0) = \mathcal{B}(\mathbf{A}_{i,j}^t; \bar{\alpha}_t \mathbf{A}_{i,j}^0). \quad (15)$$

The posterior $q(\mathbf{A}^{t-1} | \mathbf{A}^t, \mathbf{A}^0)$, whose form is discussed in Eqn. (3), is decomposed into

$$\begin{aligned} q(\mathbf{A}^{t-1} | \mathbf{A}^t, \mathbf{A}^0) &= \frac{q(\mathbf{A}^t | \mathbf{A}^{t-1}) q(\mathbf{A}^{t-1} | \mathbf{A}^0)}{q(\mathbf{A}^t | \mathbf{A}^0)} \\ &= \prod_{i,j: i < j} \frac{q(\mathbf{A}_{i,j}^t | \mathbf{A}_{i,j}^{t-1}) q(\mathbf{A}_{i,j}^{t-1} | \mathbf{A}_{i,j}^0)}{q(\mathbf{A}_{i,j}^t | \mathbf{A}_{i,j}^0)} \\ &= \prod_{i,j: i < j} q(\mathbf{A}_{i,j}^{t-1} | \mathbf{A}_{i,j}^t, \mathbf{A}_{i,j}^0) \end{aligned} \quad (16)$$

The entry-wise posterior distribution $q(\mathbf{A}_{i,j}^{t-1} | \mathbf{A}_{i,j}^t, \mathbf{A}_{i,j}^0)$ is the key identity for deriving the active node distribution. Here, we describe the detailed form of this distribution. For any value $p \in [0, 1]$, we have the form

$$q(\mathbf{A}_{i,j}^{t-1} | \mathbf{A}_{i,j}^t, \mathbf{A}_{i,j}^0) = \mathcal{B}(\mathbf{A}_{i,j}^{t-1}; \frac{p_1}{p_0 + p_1}), \text{ where} \quad (17)$$

$$p_1 = [(1 - \beta_t + \beta_t p) \mathbf{A}_{i,j}^t + (\beta_t - \beta_t p)(1 - \mathbf{A}_{i,j}^t)][\bar{\alpha}_{t-1} \mathbf{A}_{i,j}^0 + (1 - \bar{\alpha}_{t-1})p] \quad (18)$$

$$p_0 = [(\beta_t p) \mathbf{A}_{i,j}^t + (1 - \beta_t p)(1 - \mathbf{A}_{i,j}^t)][1 + \bar{\alpha}_{t-1} p - \bar{\alpha}_{t-1} \mathbf{A}_{i,j}^0 - p] \quad (19)$$

Note that the posterior derived in Sohl-Dickstein et al. (2015); Hoogeboom et al. (2021) is only applicable to the case where $p = 0.5$, the above posterior is more general. In particular, for $p = 0$ in our case, the posterior can be simplified into the following three cases

$$q(\mathbf{A}_{i,j}^{t-1} | \mathbf{A}_{i,j}^t, \mathbf{A}_{i,j}^0) = \begin{cases} \mathcal{B}(\mathbf{A}_{i,j}^{t-1}; 0), & \mathbf{A}_{i,j}^0 = 0 \\ \mathcal{B}(\mathbf{A}_{i,j}^{t-1}; 1), & \mathbf{A}_{i,j}^0 = 1, \mathbf{A}_{i,j}^t = 1 \\ \mathcal{B}(\mathbf{A}_{i,j}^{t-1}; \frac{\beta_t \bar{\alpha}_{t-1}}{1 - \bar{\alpha}_t}), & \mathbf{A}_{i,j}^0 = 1, \mathbf{A}_{i,j}^t = 0 \end{cases} \quad (20)$$

We provide an intuitive interpretation of the three cases. Since we are considering an edge-removing process, for the case where $\mathbf{A}_{i,j}^0 = 0$, the probability an edge (i, j) is formed at timestep $t - 1$ is 0 (note that the event $(\mathbf{A}_{i,j}^0 = 0, \mathbf{A}_{i,j}^t = 1)$ is unlikely to happen). The case where $\mathbf{A}_{i,j}^0 = \mathbf{A}_{i,j}^t = 1$ indicates the edge (i, j) is not removed for all timesteps from 0 to t , therefore, $\mathbf{A}_{i,j}^{t-1}$ always equals to 1. The last case is the only case with uncertainty since an edge (i, j) can be removed at any timestep before t .

A.2. Derivation of Active Node Distribution

We now have the entry-wise forward distribution and posterior distribution. We can quantify how on average, a node may have a degree change at each timestep, forward and backward. Here we first discuss the form of the forward and posterior degree distributions, which can be directly applied to calculate the degree change distributions:

Property 1. The forward degree distributions have the form

$$q(\mathbf{d}^t | \mathbf{d}^0) = \prod_{i=1}^N q(\mathbf{d}_i^t | \mathbf{d}_i^0), \text{ where } q(\mathbf{d}_i^t | \mathbf{d}_i^0) = \text{Binomial}(k = \mathbf{d}_i^t, n = \mathbf{d}_i^0, p = \bar{\alpha}_t). \quad (21)$$

$$q(\mathbf{d}^t | \mathbf{d}^{t-1}) = \prod_{i=1}^N q(\mathbf{d}_i^t | \mathbf{d}_i^{t-1}), \text{ where } q(\mathbf{d}_i^t | \mathbf{d}_i^{t-1}) = \text{Binomial}(k = \mathbf{d}_i^t, n = \mathbf{d}_i^{t-1}, p = 1 - \beta_t). \quad (22)$$

Intuitively, for $q(\mathbf{d}^t | \mathbf{d}^0)$, there are \mathbf{d}_i^0 edges connected to node i , each with probability $\bar{\alpha}_t$ to be kept at timestep t . The probability the number of remaining edges equals \mathbf{d}_i^t at timestep t is a binomial distribution. A similar statement also holds for the one-step transition $q(\mathbf{d}^t | \mathbf{d}^{t-1})$, where an edge will have probability $1 - \beta_t$ be kept when transiting from $t-1$ to t .

Since we are interested in the reverse process, we also want to derive the reverse degree distribution $q(\mathbf{d}^{t-1} | \mathbf{d}^t)$, which is intractable to compute in general. We show that this is computable when conditioning on the initial degree sequence \mathbf{d}^0 . First, we show that $q(\mathbf{d}^{t-1} | \mathbf{d}^t, \mathbf{d}^0) = q(\mathbf{d}^{t-1} | \mathbf{A}^t, \mathbf{A}^0)$ by showing $q(\mathbf{s}_i^t | \mathbf{d}_i^t, \mathbf{d}_i^0) = q(\mathbf{s}_i^t | \mathbf{A}_{i,:}^t, \mathbf{A}_{i,:}^0)$. Specifically, for each node i , we have the following derivation:

$$\begin{aligned} q(\mathbf{d}_i^{t-1} | \mathbf{A}_{i,:}^t, \mathbf{A}_{i,:}^0) &= \binom{(\mathbf{A}_{i,:}^0 - \mathbf{A}_{i,:}^t) \mathbf{1}}{\mathbf{d}_i^{t-1} - \mathbf{A}_{i,:}^t \mathbf{1}} \left(\frac{\beta_t \bar{\alpha}_{t-1}}{1 - \bar{\alpha}_t} \right)^{\mathbf{d}_i^{t-1} - \mathbf{A}_{i,:}^t \mathbf{1}} \cdot \left(\frac{1 - \bar{\alpha}_{t-1}}{1 - \bar{\alpha}_t} \right)^{(\mathbf{A}_{i,:}^0 - \mathbf{A}_{i,:}^t) \mathbf{1} - (\mathbf{d}_i^{t-1} - \mathbf{A}_{i,:}^t \mathbf{1})} \\ &= \binom{\mathbf{d}_i^0 - \mathbf{d}_i^t}{\mathbf{d}_i^{t-1} - \mathbf{d}_i^t} \left(\frac{\beta_t \bar{\alpha}_{t-1}}{1 - \bar{\alpha}_t} \right)^{\mathbf{d}_i^{t-1} - \mathbf{d}_i^t} \cdot \left(\frac{1 - \bar{\alpha}_{t-1}}{1 - \bar{\alpha}_t} \right)^{(\mathbf{d}_i^0 - \mathbf{d}_i^t) - (\mathbf{d}_i^{t-1} - \mathbf{d}_i^t)} \\ &= (\mathbf{d}_i^{t-1} | \mathbf{d}_i^t, \mathbf{d}_i^0) \end{aligned} \quad (23)$$

The posterior degree distribution is also binomial. From Eqn. (20), we know that only when $\mathbf{A}_{i,j}^0 = 1$ and $\mathbf{A}_{i,j}^t = 0$, there is uncertainty in the edge posterior distribution. The number of such edges incident to node i is $\mathbf{d}_i^0 - \mathbf{d}_i^t$, yielding a binomial distribution with $\mathbf{d}_i^0 - \mathbf{d}_i^t$ trials, each trial with Bernoulli parameter $\frac{\beta_t \bar{\alpha}_{t-1}}{1 - \bar{\alpha}_t}$. Now we summarize the posterior degree distribution into the property below:

Property 2. The posterior degree distribution has the form

$$\begin{aligned} q(\mathbf{d}^{t-1} | \mathbf{d}^t, \mathbf{d}^0) &= \prod_{i=1}^N q(\mathbf{d}_i^{t-1} | \mathbf{d}_i^t, \mathbf{d}_i^0), \text{ where} \\ q(\mathbf{d}_i^{t-1} | \mathbf{d}_i^t, \mathbf{d}_i^0) &= \text{Binomial}(k = \Delta_i^t, n = \Delta_i^0, p = \gamma_t), \\ \text{with } \Delta_i^t &= \mathbf{d}_i^{t-1} - \mathbf{d}_i^t, \Delta_i^0 = \mathbf{d}_i^0 - \mathbf{d}_i^t, \gamma_t = \frac{\beta_t \bar{\alpha}_{t-1}}{1 - \bar{\alpha}_t}. \end{aligned} \quad (24)$$

Now we have derived the forward and reverse degree distributions. It's obvious that when a node has no degree change from timestep $t-1$ to t or the other way around, we always have $\mathbf{d}_i^{t-1} = \mathbf{d}_i^t$. The probabilities of such events can be computed by querying the degree distributions $q(\mathbf{d}^t | \mathbf{d}^{t-1})$ or $q(\mathbf{d}^{t-1} | \mathbf{d}^t, \mathbf{d}^0)$. Let \mathbf{s}_i^t be the random variable that node i has degree change at timestep t . Below we show the forward and reverse degree change distributions:

Property 3. At timestep t , the forward degree change distribution for node i given \mathbf{d}_i^{t-1} is

$$q(\mathbf{s}_i^t | \mathbf{d}_i^{t-1}) = \mathcal{B}(\mathbf{s}_i^t; 1 - \beta_t^{\mathbf{d}_i^{t-1}}). \quad (25)$$

Property 4. At timestep t , the reverse degree change distribution for node i given $\mathbf{d}_i^t, \mathbf{d}_i^0$ is

$$q(\mathbf{s}_i^t | \mathbf{d}_i^t, \mathbf{d}_i^0) = \mathcal{B}(\mathbf{s}_i^t; 1 - (1 - \gamma_t)^{\Delta_i^0}). \quad (26)$$

The forward degree change distribution provides insightful supporting evidence that only a part of nodes may have degree change at each transition, motivating us the develop such a scalable generative framework. Controlling the number of nodes with degree change in the forward process can function as a principle to improve the noise scheduling algorithm. In practice, we only use the reverse degree change distribution when learning the reverse process. The reverse degree distribution is essential in improving the model expressivity since it enables graph generation with degree guidance.

B. Derivations of the Training Objectives

B.1. Derivation of the objective $\mathcal{L}(\mathbf{A}^0; \theta)$

To obtain the objective $\mathcal{L}(\mathbf{A}^0; \theta)$, we first need to derive the posterior of \mathbf{A}^{t-1} that conditions on the introduced latent variables \mathbf{s}^t

$$\begin{aligned} q(\mathbf{A}^{t-1} | \mathbf{A}^t, \mathbf{s}^t, \mathbf{A}^0) &= \frac{q(\mathbf{A}^{t-1}, \mathbf{A}^t, \mathbf{s}^t | \mathbf{A}^0)}{q(\mathbf{A}^t, \mathbf{s}^t | \mathbf{A}^0)} \\ &= \frac{q(\mathbf{A}^t | \mathbf{A}^{t-1}, \mathbf{A}^0)q(\mathbf{s}^t | \mathbf{A}^t, \mathbf{A}^{t-1}, \mathbf{A}^0)q(\mathbf{A}^{t-1} | \mathbf{A}^0)}{q(\mathbf{A}^t, \mathbf{s}^t | \mathbf{A}^0)} \\ &= \frac{q(\mathbf{A}^t | \mathbf{A}^{t-1})q(\mathbf{s}^t | \mathbf{A}^t, \mathbf{A}^{t-1})q(\mathbf{A}^{t-1} | \mathbf{A}^0)}{q(\mathbf{A}^t | \mathbf{A}^0)q(\mathbf{s}^t | \mathbf{A}^t, \mathbf{A}^0)}. \end{aligned} \quad (27)$$

By rearranging terms, we have

$$q(\mathbf{A}^t | \mathbf{A}^{t-1})q(\mathbf{s}^t | \mathbf{A}^t, \mathbf{A}^{t-1}) = \frac{q(\mathbf{A}^{t-1} | \mathbf{A}^t, \mathbf{s}^t, \mathbf{A}^0)q(\mathbf{A}^t | \mathbf{A}^0)q(\mathbf{s}^t | \mathbf{A}^t, \mathbf{A}^0)}{q(\mathbf{A}^{t-1} | \mathbf{A}^0)}. \quad (28)$$

The VLB $\mathcal{L}(\mathbf{A}^0; \theta)$ of $\log p(\mathbf{A}^0)$ is derived as follow

$$\begin{aligned} &\mathcal{L}(\mathbf{A}^0; \theta) \\ &= \mathbb{E}_q \left[\log \frac{p_\theta(\mathbf{A}^{0:T}, \mathbf{s}^{1:T})}{q(\mathbf{A}^{1:T}, \mathbf{s}^{1:T} | \mathbf{A}^0)} \right] \\ &= \mathbb{E}_q \left[\log \frac{p(\mathbf{A}^T) \prod_{t=1}^T p_\theta(\mathbf{A}^{t-1}, \mathbf{s}^t | \mathbf{A}^t)}{\prod_{t=1}^T q(\mathbf{A}^t, \mathbf{s}^t | \mathbf{A}^{t-1})} \right] \\ &= \mathbb{E}_q \left[\log p(\mathbf{A}^T) + \sum_{t=1}^T \log \frac{p_\theta(\mathbf{A}^{t-1} | \mathbf{A}^t, \mathbf{s}^t) p_\theta(\mathbf{s}^t | \mathbf{A}^t)}{q(\mathbf{A}^t | \mathbf{A}^{t-1}) q(\mathbf{s}^t | \mathbf{A}^t, \mathbf{A}^{t-1})} \right] \\ &= \mathbb{E}_q \left[\log p(\mathbf{A}^T) + \log \frac{p_\theta(\mathbf{A}^0 | \mathbf{A}^1, \mathbf{s}^1) p_\theta(\mathbf{s}^1 | \mathbf{A}^1)}{q(\mathbf{A}^1 | \mathbf{A}^0) q(\mathbf{s}^1 | \mathbf{A}^1, \mathbf{A}^0)} + \sum_{t=2}^T \log \frac{p_\theta(\mathbf{A}^{t-1} | \mathbf{A}^t, \mathbf{s}^t) p_\theta(\mathbf{s}^t | \mathbf{A}^t)}{\frac{q(\mathbf{A}^{t-1} | \mathbf{A}^t, \mathbf{s}^t, \mathbf{A}^0) q(\mathbf{A}^t | \mathbf{A}^0) q(\mathbf{s}^t | \mathbf{A}^t, \mathbf{A}^0)}{q(\mathbf{A}^{t-1} | \mathbf{A}^0)}} \right] \\ &= \mathbb{E}_q \left[\log p(\mathbf{A}^T) + \log \frac{p_\theta(\mathbf{A}^0 | \mathbf{A}^1, \mathbf{s}^1) p_\theta(\mathbf{s}^1 | \mathbf{A}^1)}{q(\mathbf{A}^1 | \mathbf{A}^0) q(\mathbf{s}^1 | \mathbf{A}^1, \mathbf{A}^0)} + \sum_{t=2}^T \log \frac{p_\theta(\mathbf{A}^{t-1} | \mathbf{A}^t, \mathbf{s}^t) p_\theta(\mathbf{s}^t | \mathbf{A}^t) q(\mathbf{A}^{t-1} | \mathbf{A}^0)}{q(\mathbf{A}^{t-1} | \mathbf{A}^t, \mathbf{s}^t, \mathbf{A}^0) q(\mathbf{s}^t | \mathbf{A}^t, \mathbf{A}^0) q(\mathbf{A}^t | \mathbf{A}^0)} \right] \\ &= \mathbb{E}_q \left[\log \frac{p(\mathbf{A}^T) q(\mathbf{A}^T | \mathbf{A}^0)}{q(\mathbf{A}^T | \mathbf{A}^0)} + \log \frac{p_\theta(\mathbf{A}^0 | \mathbf{A}^1, \mathbf{s}^1) p_\theta(\mathbf{s}^1 | \mathbf{A}^1)}{\cancel{q(\mathbf{A}^1 | \mathbf{A}^0)} q(\mathbf{s}^1 | \mathbf{A}^1, \mathbf{A}^0)} + \sum_{t=2}^T \log \frac{p_\theta(\mathbf{A}^{t-1} | \mathbf{A}^t, \mathbf{s}^t) p_\theta(\mathbf{s}^t | \mathbf{A}^t) q(\mathbf{A}^{t-1} | \mathbf{A}^0)}{q(\mathbf{A}^{t-1} | \mathbf{A}^t, \mathbf{s}^t, \mathbf{A}^0) q(\mathbf{s}^t | \mathbf{A}^t, \mathbf{A}^0) q(\mathbf{A}^t | \mathbf{A}^0)} \right] \\ &= \mathbb{E}_q \left[\log \frac{p(\mathbf{A}^T)}{q(\mathbf{A}^T | \mathbf{A}^0)} + \underbrace{\log p_\theta(\mathbf{A}^0 | \mathbf{A}^1, \mathbf{s}^1)}_{\text{reconstruction term } \mathcal{L}_{\text{rec}}} + \sum_{t=2}^T \underbrace{\log \frac{p_\theta(\mathbf{A}^{t-1} | \mathbf{A}^t, \mathbf{s}^t)}{q(\mathbf{A}^{t-1} | \mathbf{A}^t, \mathbf{s}^t, \mathbf{A}^0)}}_{\text{edge prediction term } \mathcal{L}_{\text{edge}}(t)} + \sum_{t=1}^T \underbrace{\log \frac{p_\theta(\mathbf{s}^t | \mathbf{A}^t)}{q(\mathbf{s}^t | \mathbf{A}^t, \mathbf{A}^0)}}_{\text{node selection term } \mathcal{L}_{\text{node}}(t)} \right]. \end{aligned} \quad (29)$$

The objective requires modeling two latent variables: $\mathbf{A}^{1:T}$ and $\mathbf{s}^{1:T}$. Learning to predict \mathbf{s}^t from \mathbf{A}^t can be difficult since it involves capturing the dynamic interaction between nodes and the global structure of the current graph \mathbf{A}^t . In Section B.2, we demonstrate a new objective which can avoid learning $p_\theta(\mathbf{s}^t | \mathbf{A}^t)$ by instead learning the node degree distribution $p_\theta(\mathbf{d}^0)$.

B.2. Derivation of the objective $\mathcal{L}(\mathbf{A}^0, \mathbf{d}^0; \theta)$

Since $p_\theta(\mathbf{A}^0) = p_\theta(\mathbf{A}^0, \mathbf{d}^0)$, we have

$$\begin{aligned}
 \log p_\theta(\mathbf{A}^0) &= \log p_\theta(\mathbf{A}^0, \mathbf{d}^0) \geq \mathcal{L}(\mathbf{A}^0, \mathbf{d}^0; \theta) \\
 &= \mathbb{E}_q \left[\log \frac{p_\theta(\mathbf{d}^0) p_\theta(\mathbf{A}^0 | \mathbf{d}^0)}{q(\mathbf{d}^0 | \mathbf{A}^0) q(\mathbf{A}^{1:T} | \mathbf{A}^0)} \right] \\
 &= \mathbb{E}_q \left[\log \frac{p_\theta(\mathbf{d}^0) p_\theta(\mathbf{A}^{0:T}, \mathbf{s}^{1:T} | \mathbf{d}^0)}{q(\mathbf{d}^0 | \mathbf{A}^0) q(\mathbf{A}^{1:T}, \mathbf{s}^{1:T} | \mathbf{A}^0)} \right] \\
 &= \underbrace{\mathbb{E}_q \left[\log \frac{p_\theta(\mathbf{d}^0)}{q(\mathbf{d}^0 | \mathbf{A}^0)} \right]}_{\mathcal{L}(\mathbf{d}^0; \theta)} + \underbrace{\mathbb{E}_q \left[\log \frac{p_\theta(\mathbf{A}^{0:T}, \mathbf{s}^{1:T} | \mathbf{d}^0)}{q(\mathbf{A}^{1:T}, \mathbf{s}^{1:T} | \mathbf{A}^0)} \right]}_{\mathcal{L}(\mathbf{A}^0 | \mathbf{d}^0; \theta)}.
 \end{aligned} \tag{30}$$

Optimizing $\mathcal{L}(\mathbf{d}^0; \theta)$ is equivalent to fitting $p_\theta(\mathbf{d}^0)$ to the node degree data distribution $p_{\text{data}}(\mathbf{d}^0)$ as \mathbf{d}^0 is obtained from \mathbf{A}^0 . The full decomposition of $\mathcal{L}(\mathbf{A}^0 | \mathbf{d}^0; \theta)$ has the following form:

$$\mathcal{L}(\mathbf{A}^0 | \mathbf{d}^0; \theta) = \mathbb{E}_q \left[\log \frac{p(\mathbf{A}^T)}{q(\mathbf{A}^T | \mathbf{A}^0)} + \underbrace{\log p_\theta(\mathbf{A}^0 | \mathbf{A}^1, \mathbf{s}^1, \mathbf{d}^0)}_{\text{reconstruction term } \mathcal{L}_{\text{rec}}} + \sum_{t=2}^T \underbrace{\log \frac{p_\theta(\mathbf{A}^{t-1} | \mathbf{A}^t, \mathbf{s}^t, \mathbf{d}^0)}{q(\mathbf{A}^{t-1} | \mathbf{A}^t, \mathbf{s}^t, \mathbf{A}^0)}}_{\text{edge prediction term } \mathcal{L}_{\text{edge}}(t)} + \sum_{t=1}^T \underbrace{\log \frac{p_\theta(\mathbf{s}^t | \mathbf{A}^t, \mathbf{d}^0)}{q(\mathbf{s}^t | \mathbf{A}^t, \mathbf{A}^0)}}_{\text{node selection term } \mathcal{L}_{\text{node}}(t)} \right]. \tag{31}$$

Here \mathbf{A}^T is independent from \mathbf{d}^0 so $p(\mathbf{A}^T | \mathbf{d}^0) = p(\mathbf{A}^T)$. And as mentioned before, we choose to parameterize $p_\theta(\mathbf{s}^t | \mathbf{A}^t, \mathbf{d}^0) := q(\mathbf{s}^t | \mathbf{A}^t, \mathbf{A}^0)$, resulting in the KL divergence $\mathcal{L}_{\text{node}}(t) = 0$ for all t . The objective is further simplified to

$$\mathcal{L}(\mathbf{A}^0 | \mathbf{d}^0; \theta) = \mathbb{E}_q \left[\log \frac{p(\mathbf{A}^T)}{q(\mathbf{A}^T | \mathbf{A}^0)} + \log p_\theta(\mathbf{A}^0 | \mathbf{A}^1, \mathbf{s}^1, \mathbf{d}^0) + \sum_{t=2}^T \log \frac{p_\theta(\mathbf{A}^{t-1} | \mathbf{A}^t, \mathbf{s}^t, \mathbf{d}^0)}{q(\mathbf{A}^{t-1} | \mathbf{A}^t, \mathbf{s}^t, \mathbf{A}^0)} \right]. \tag{32}$$

C. Detailed Implementations of the Denoising Networks and Training

C.1. Parameterization of the edge prediction distribution

As we consider modeling the upper triangle of the adjacency matrix, the edge prediction distribution $p_\theta(\mathbf{A}^{t-1} | \mathbf{A}^t, \mathbf{s}^t, \mathbf{d}^0)$ is parameterized as:

$$\begin{aligned}
 p_\theta(\mathbf{A}^{t-1} | \mathbf{A}^t, \mathbf{s}^t, \mathbf{d}^0) &= \prod_{i,j: i < j} p_\theta(\mathbf{A}_{i,j}^{t-1} | \mathbf{A}_{i,j}^t, \mathbf{s}_{i,j}^t, \mathbf{d}^0), \text{ with} \\
 p_\theta(\mathbf{A}_{i,j}^{t-1} | \mathbf{A}_{i,j}^t, \mathbf{s}_{i,j}^t, \mathbf{d}^0) &= \mathcal{B}(\mathbf{A}_{i,j}^t; \mathbf{s}_{i,j}^t \ell_{i,j}^{t-1} + (1 - \mathbf{s}_{i,j}^t) \mathbf{A}_{i,j}^t), \\
 \text{where } \mathbf{s}_{i,j}^t &= \mathbf{s}_i^t \mathbf{s}_j^t, \ell^{t-1} = \text{gnn}_\theta(\mathbf{A}^t, \mathbf{s}^t, \mathbf{d}^0, t).
 \end{aligned} \tag{33}$$

Note that only when nodes i, j are both selected, i.e., $\mathbf{s}_{i,j}^t = 1$, the corresponding Bernoulli parameter $\ell_{i,j}^{t-1}$ effectively decides the edge distribution. Below we elaborate on the architecture of the used network and analyze the runtime complexity.

Architecture design and complexity analysis. Figure 5 shows the parameterization and the inference procedure of the edge prediction model. The main component of the parameterized network consists of L message-passing blocks (MPB). After constructing the inputs, we iteratively update the node features using MPBs, and then compute the Bernoulli parameter $\ell_{i,j}^{t-1}$ for node pairs (i, j) using a Multilayer perceptron(MLP). The computation flow is shown below

$$\begin{aligned}
 \mathbf{Z}^0 &= \text{concat}(\text{emb}(\mathbf{d}^t) \| \text{emb}(\mathbf{d}^0)), \mathbf{t}_{\text{emb}} = \text{emb}(t), \mathbf{c}^0 = \text{mean}(\mathbf{Z}^0); \\
 \mathbf{Z}^l, \mathbf{c}^l, \mathbf{H}^l &= \text{block}_l(\mathbf{Z}^{l-1}, \mathbf{t}_{\text{emb}}, \mathbf{c}^{l-1}, \mathbf{H}^{l-1}), \text{ for } l = 1, \dots, L; \\
 \ell_{i,j}^{t-1} &= \text{mlp}(\mathbf{Z}_i^L + \mathbf{Z}_j^L), \text{ where } (i, j) \in \{(i, j) | \mathbf{s}_{i,j}^t = 1, 1 \leq i < j \leq N\}.
 \end{aligned}$$

Here \mathbf{Z}^0 is the node features initialized using degree sequence \mathbf{d}^0 and \mathbf{d}^t ; \mathbf{c} is the global context features; \mathbf{H} is the node hidden state features. We follow Dhariwal & Nichol (2021) and use the sinusoidal position embedding for the diffusion

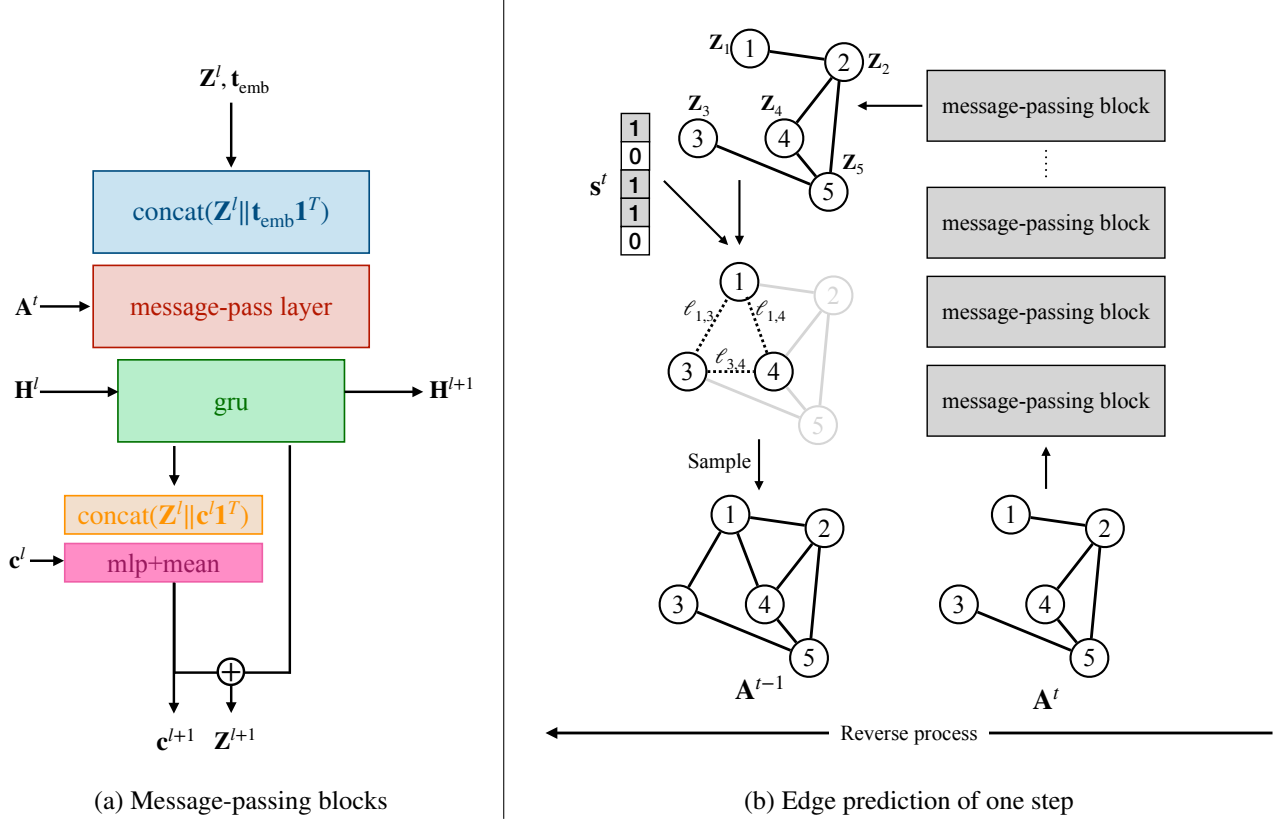


Figure 5. Parameterization and inference of the edge prediction network. (a) shows the architecture of an MPB, which updates the node features \mathbf{Z} and context feature \mathbf{c} via message-passing. The state vectors \mathbf{H} are used for keeping geometric information at different levels of layers. (b) shows how the model infers edges during the reverse process. The node features are computed using a stacked MPB. The model only predicts edges between active nodes indicated by \mathbf{s}^t .

timestep t . \mathbf{Z} , \mathbf{c} , and \mathbf{H} are iteratively updated by MPBs. Finally, the edge prediction parameter $\ell_{i,j}^{t-1}$ is computed from the two node embeddings.

Each MPB contains a message-passing layer (MPL) and a Gated Recurrent Unit (GRU) (Cho et al., 2014). We experimented on various MPLs and found Unified Message Passaging Model (Shi et al., 2020) demonstrates better expressivity for our tasks. The details for the l -th MPB can be represented as follow

$$\begin{aligned}
 \mathbf{Z}^l &= \text{concat}(\mathbf{Z}^l \parallel \mathbf{t}_{\text{emb}} \mathbf{1}^T) \\
 \mathbf{Z}^l &= \text{mpl}(\mathbf{Z}^l, \mathbf{A}^t) \\
 \mathbf{Z}^l, \mathbf{H}^{l+1} &= \text{gru}(\mathbf{Z}^l, \mathbf{H}^l) \\
 \mathbf{c}^{l+1} &= \text{mlp}(\text{mean}(\text{concat}(\mathbf{Z}^l \parallel \mathbf{c}^l \mathbf{1}^T))) \\
 \mathbf{Z}^{l+1} &= \mathbf{Z}^l + \mathbf{c}^{l+1} \mathbf{1}^T
 \end{aligned}$$

Note that in MPB, the message-passing operation has runtime complexity $O(M)$, and all other operations have runtime complexity $O(N)$ as they operate on node features. The total runtime complexity of an MPB module is $O(M)$. Another major computation comes from the edge probability predictions, which are decided by the size of the node-pair set $|\{(i, j) | \mathbf{s}_{i,j}^t = 1, i < j\}| = (\sum_i \mathbf{s}_i^t)^2 \leq K^2$.

C.2. Modeling the degree sequence distribution

We want the generative model $p_\theta(\mathbf{d}^0)$ is invariant on node permutation π , i.e., for all π , we have $p_\theta(\mathbf{d}^0) = p_\theta(\pi(\mathbf{d}^0))$. Let $\mathbf{u} \in \{0, \dots, N_{\max}\}^{d_{\max}}$ be a histogram such that $\mathbf{u}_k = \sum_{i=1}^N \mathbf{1}[\mathbf{d}_i^0 = k]$ for $k = 1, \dots, d_{\max}$, and d_{\max} is the maximum

node degree in the graph training set. We consider modeling $q(\mathbf{u}|\mathbf{A}^0)$ instead of $q(\mathbf{d}^0|\mathbf{A}^0)$ as \mathbf{u} is invariant to node permutation. The training objective is then to fit $p_\theta(\mathbf{u})$ to the empirical data distribution $p_{\text{data}}(\mathbf{u})$. We consider it a sequence modeling task. The model $p_\theta(\mathbf{u})$ has the following decomposition

$$p_\theta(\mathbf{u}) = p_\theta(\mathbf{u}_1|\text{SOS}) \prod_{k=2}^{d_{\max}} p_\theta(\mathbf{u}_k|\mathbf{u}_{<k}). \quad (34)$$

We parameterize $p_\theta(\mathbf{u}_k|\mathbf{u}_{<k})$ with a RNN (Schuster & Paliwal, 1997), where the RNN produces N_{\max} -dimensional softmax logits at each step. SOS is a start token used at the beginning of the generation. Once a sequence \mathbf{u} is sampled, the graph's corresponding size is known. Note that we only model the degree distribution for the generic graph generation task. We only have one graph for large network generation for each dataset. We use the node degrees of the training graph when sampling new graphs. We describe the sampling algorithm in Alg. 2.

Algorithm 2 Sampling the degree sequence \mathbf{d}^0

Input: Maximum degree d_{\max} , degree sequence model $p_\theta(\mathbf{u})$.
 Draw $\mathbf{u}_1 \sim p_\theta(\mathbf{u}_1|\text{SOS})$, initialize \mathbf{d}^0 as an empty vector.
for $k = 2, \dots, d_{\max}$ **do**
 Initialize \mathbf{u}_k -dimensional all-ones vector $\mathbf{1}^k$, set $\mathbf{d}^0 = \text{concat}(\mathbf{d}^0 \| k\mathbf{1}^k)$.
 Draw $\mathbf{u}_k \sim p_\theta(\mathbf{u}_k|\mathbf{u}_{<k})$
end for
Output: Degree sequence \mathbf{d}^0

C.3. Training

We demonstrate the training of the edge prediction model $p_\theta(\mathbf{A}^{t-1}|\mathbf{A}^t, \mathbf{s}^t, \mathbf{d}^0)$. Since we do not have the closed-form for $q(\mathbf{A}^{t-1}|\mathbf{A}^t, \mathbf{s}^t, \mathbf{A}^0)$, the gradient $\nabla_\theta \mathcal{L}(\mathbf{A}^0; \theta, \mathbf{d}^0)$ is estimated via full Monte Carlo,

$$\nabla_\theta \mathcal{L}(\mathbf{A}^0; \theta, \mathbf{d}^0) = \mathbb{E}_{t \sim \mathcal{U}[1, T]} \left[\mathbb{E}_{q(\mathbf{A}^{t-1}|\mathbf{A}^0)} \mathbb{E}_{q(\mathbf{A}^t|\mathbf{A}^{t-1})} \mathbb{E}_{q(\mathbf{s}^t|\mathbf{A}^{t-1}, \mathbf{A}^t)} \left[\log p_\theta(\mathbf{A}^t|\mathbf{A}^{t-1}, \mathbf{s}^t, \mathbf{d}^0) \right] \right]. \quad (35)$$

We describe the procedure of training the edge prediction model in Alg. 3

Algorithm 3 Training procedure for edge prediction model

Input: Data distribution $p_{\text{data}}(\mathbf{A}^0)$, diffusion steps T , forward transition distributions $q(\mathbf{A}^t|\mathbf{A}^{t-1})$ and $q(\mathbf{A}^t|\mathbf{A}^0)$.
while training **do**
 Draw $\mathbf{A}^0 \sim p_{\text{data}}(\mathbf{A}^0)$, and $t \sim \mathcal{U}[1, T]$.
 Draw $\mathbf{A}^{t-1} \sim q(\mathbf{A}^{t-1}|\mathbf{A}^0)$, then draw $\mathbf{A}^t \sim q(\mathbf{A}^t|\mathbf{A}^{t-1})$.
 Obtain active node variable \mathbf{s}^t from $\mathbf{A}^{t-1}, \mathbf{A}^t$, and compute node degree $\mathbf{d}^0 = \deg(\mathbf{A}^0)$.
 Perform gradient descent over θ with gradient $\nabla_\theta \log p_\theta(\mathbf{A}^t|\mathbf{A}^{t-1}, \mathbf{s}^t, \mathbf{d}^0)$
end while

D. Further Discussion of Current Diffusion Graph Models

D.1. Technical differences of existing diffusion-based graph models

Diffusion-based generative models (Sohl-Dickstein et al., 2015; Ho et al., 2020; Hoogeboom et al., 2021; Austin et al., 2021) have gained prominent attention in the graph generation community. Current diffusion graph models adopt continuous or discrete-variable diffusion. For example, GDSS (Jo et al., 2022) and EDP-GNN (Niu et al., 2020) use Gaussian transition kernels for continuous-variable diffusion (Ho et al., 2020), but GDSS additionally considers node and edge features and uses a score-matching diffusion approach. On the other hand, DiscDDPM (Haefeli et al., 2022) and DiGress (Vignac et al., 2022) employ discrete-time, discrete-variable diffusion models (Hoogeboom et al., 2021; Austin et al., 2021), with the former being featureless and the latter including a denoising process for node and edge attributes.

One limitation shared by all current diffusion graph models is suffering from the scalability issue: they all need $O(TN^2)$ running time because they need to make predictions for each node pair in each diffusion step. This limitation prevents diffusion graph models from generating large networks. The main advantage of EDGE is to reduce this complexity to $O(\min(K^2, M))$, with K being the number of active nodes and M being the number of edges. It greatly reduces the computation in the generation process and has shown promising results in large network generation tasks. We further highlight the limitation and technical differences of different models in Table 7.

	Diffusion type	Convergent distribution	Conditional generation	Featured graph generation	Runtime	Scalability
EDP-GNN	Disc. time, Cont. var.	$\mathcal{N}(0, 1)$			$O(TN^2)$	
GDSS	Cont. time, Cont. var.	$\mathcal{N}(0, 1)$		✓	$O(TN^2)$	
DiscDDPM	Disc. time, Disc. var.	$G(N, 0.5)$			$O(TN^2)$	
DiGress	Disc. time, Disc. var.	Empirical distribution	Gradient from a classifier	✓	$O(TN^2)$	
EDGE (ours)	Disc. time, Disc. var.	$G(N, 0)$	degree sequence		$O(T \max(M, K^2))$	✓

Table 7. Technical differences of different diffusion graph models. Here T is the number of diffusion steps, N is the number of nodes in a graph, M is the number of edges in a graph, and K is the maximum number of active nodes during the diffusion process.

E. Generalizing to Featured Graph Generation

E.1. Hierarchical generation

Featured graph generation has a broad class of applications, such as molecule generation (Du et al., 2021). It is intriguing if a graph generative model can be used to generate such graphs. While EDGE is developed to generate graph structure only, here we briefly discuss how it can be incorporated into a hierarchical procedure to generate graphs with node and edge features. Here we consider the case where node and edge attributes are both categorical data.

The attributes of nodes and edges are represented using a one-hot encoded format. For node attributes, we have a matrix $\mathbf{X} \in \{0, 1\}^{N \times C_{\text{node}}}$, while edge attributes are described by the matrix $\mathbf{A}_{\text{attr}} \in \{0, 1\}^{N \times (C_{\text{edge}} + 1)}$. In this context, C_{node} and C_{edge} denote the number of classes for node types and edge types, respectively. The graph structure is still denoted by \mathbf{A} . Inspired by Lippe & Gavves (2020), we consider the following decomposition of the joint model

$$p(\mathbf{X}, \mathbf{A}_{\text{attr}}, \mathbf{A}) = p(\mathbf{X})p(\mathbf{A}|\mathbf{X})p(\mathbf{A}_{\text{attr}}|\mathbf{X}, \mathbf{A}), \quad (36)$$

which can be considered a hierarchical generation scheme that first samples the attribute for each node from some model $p(\mathbf{X})$, then given the node attribute, we compose graph structure via EDGE and finally, we attribute each edge in \mathbf{A} .

E.2. Model Details

We consider modeling each component in Eqn. (36) separately. For $p(\mathbf{X})$, we employ a similar approach as with the node degree sequence modeling, but we use the sequence length C_{node} instead of d_{\max} . For $p(\mathbf{A}|\mathbf{X})$, we apply the EDGE framework, incorporating node features from \mathbf{X} during both the training and generation phases. For $p(\mathbf{A}_{\text{attr}}|\mathbf{X}, \mathbf{A})$, we utilize a diffusion model that starts by randomly assigning edge types to the featureless edges \mathbf{A} and iteratively refines the edge label, relying on the information given by \mathbf{X} and \mathbf{A} . It is important to note that we only refine labels for edges already specified by \mathbf{A} , allowing us to use an MPNN to calculate edge features. We adopt the framework outlined in Appendix C, and only perform prediction for predefined edges.

F. Additional Details for Experimental Setups

We described the details of the experiments of generic graph generation and large network generation tasks. We provide the hyperparameters used in the experiments in Table 8. We do not augment the data input with extra features for all generation tasks except for the current node degrees \mathbf{d}^t and the node degrees \mathbf{d}^0 , which are both computation-free. Moreover, we set $p = 10^{-12}$ in our implementation to maintain numerical stability.

	Community	Ego	Polblogs	Cora	Road-Minnesota	PPI
Diffusion						
Diffusion steps T	128	128	256	64	64	512
Noise scheduling				Linear		
β_0	7.8125×10^{-4}		3.9063×10^{-4}		1.5625×10^{-3}	1.9531×10^{-4}
β_T	1.5625×10^{-1}		7.8125×10^{-2}		3.1250×10^{-1}	3.9063×10^{-2}
Sample time method				Importance sampling		
Optimization						
Learning rate				10^{-4}		
Optimizer				Adam (Kingma & Ba, 2014)		
weight decay				10^{-4}		
Batch size	64	64	4	4	4	1
Number of epochs/iteration	30000	10000	50000	50000	50000	50000
Architecture						
Number of MPBs				5		
Hidden dimension of MPL				64		
Hidden dimension of GRU				64		
Activation function				SiLU (Elfwing et al., 2018)		
Time embedding				Sinusoidal positional embedding (Devlin et al., 2018)		
Dropout rate				0.1		
Evaluation						
Number of generated graphs	128	128	5	5	5	5
d_{\max}	40	100	351	168	5	593
Number of attention heads	8	8	8	8	8	8

Table 8. Hyperparameters

F.1. Generic graph generation

We follow You et al. (2018) to generate the Community and Ego datasets and use the same data splitting strategy. Recent works (O’Bray et al., 2021; Thompson et al., 2022) have suggested better metrics for evaluating the quality of the generated graphs. To make a fair comparison, we reproduce all baselines and follow Thompson et al. (2022) to re-evaluate their generative performance. All the baselines are reproduced using their default hyperparameter setting except for GraphCNF and DiGress. For GraphCNF, we use the same model configuration of its molecule generation task for the Community dataset and a smaller model for the Ego dataset due to the limited capacity of the GPU memory. For DiGress, we do not augment the graphs with the structural features to ensure a fair comparison is made.

F.2. Large network generation

We consider the single network for each large network dataset as the training dataset. Since the evaluation metrics do not require referring to the test graphs, we do not include validation/test sets in this task. All models are trained until the training losses no longer decrease, and the models of the final epoch are used to generate samples. For GraphRNN, we use the default BFS ordering to generate adjacency matrices for the model training. We train the model for 30000 iterations for all datasets and report the model performance using the checkpoint from the last epoch.

Computating the Edge Overlap. Since GraphRNN and our model are edge non-independent models, Chanpuriya et al. (2021) suggests reporting the maximum edge overlap between the generated graphs and the training graph to ensure the models do not simply memorize the data. However, finding the maximum edge overlap requires searching over the node permutation space, which is impractical as there are $N!$ permutations. Instead, we obtain the node degree ascending permutation and use it to permute both the generated and training graphs. We observe that such a permutation scheme yields a much higher EO value than a random permutation. For instance, when a model can generate graphs with desiring statistics, degree-based permutation yields 15% EO on average for the Poblogs dataset, while a random permutation yields an EO value that is almost 0.

F.3. Computational Resources

We use PyTorch (Paszke et al., 2019) and PyTorch Geometric (Fey & Lenssen, 2019) to implement our framework. We train our models on Tesla A100, Tesla V100, or NVIDIA QUADRO RTX 6000 GPU and 32 CPU cores for all experiments. For generic graph generation tasks, all models are trained within 72 hours. For large network generation tasks, model training is finished within 24 hours. The sampling speed reported in Figure 3 of all baselines and our approach is tested on Tesla A100 GPU.

G. Extended Results

G.1. Comparison between the node degrees from generated graphs and the node degrees d^0

We show that the generated graphs' node degrees accurately approximate the given node degrees d^0 . The node degrees in the generated graphs are compared to the node degrees d^0 by counting the number of nodes whose degree deviates from the given one. The degree difference is computed by subtracting the given degree from the actual degree. The histograms in Figure 6 display the degree difference for each dataset, indicating the accuracy of the generated graph's node degrees in approximating the given node degrees.

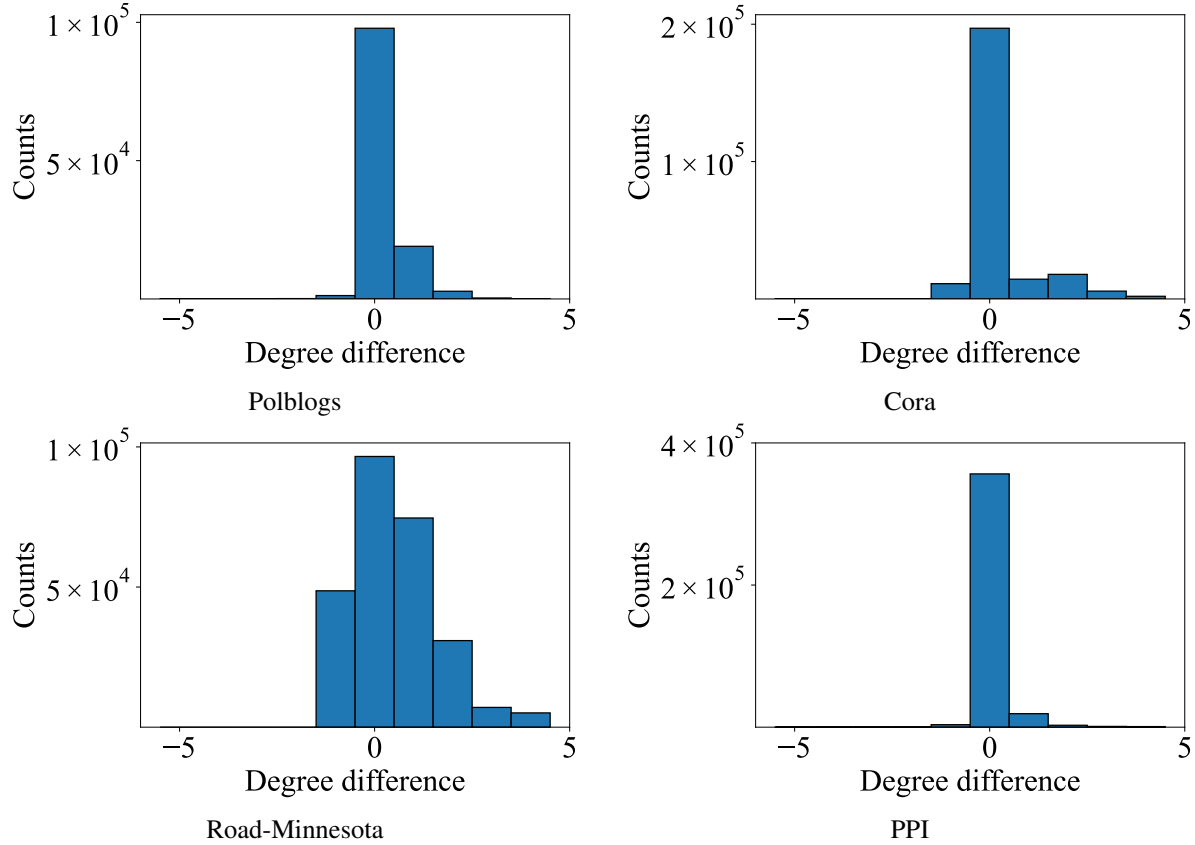


Figure 6. Degree difference. Given specific node degrees d^0 , the actual node degrees of the generated graphs are fairly accurate.

G.2. Further justification the use of $G(N, 0)$ as the convergent distribution

In addition to the desirable properties we described in Section 3.1, we demonstrate the potential benefit of using $G(N, 0)$ as the convergent distribution in terms of generative performance. When using $G(N, 0)$ as the convergent distribution, our proposed framework can be considered as a type of absorbing diffusion process (Austin et al., 2021). Similar to (Austin et al., 2021), we observe that the generative performance of $G(N, 0)$ is superior to $G(N, 0.5)$. Table 9 report the generative performance of $G(N, 0.5)$ and $G(N, 0)$ on the Community-small dataset (You et al., 2018). This demonstrates the superiority of using an absorbing state as the convergent distribution, which further justifies why one should consider

$G(N, 0)$ as the convergent distribution.

Community-small					
	Structure-based metrics (MMD)			Neural-based metrics	
	Deg.	Clus.	Orb.	FID	RBF MMD
$G(N, 0.5)$	0.0274	0.0249	0.0234	3.4121	0.0243
$G(N, 0)$	0.0081	0.0112	0.0262	1.5642	0.0204

Table 9. Vanilla discrete diffusion with $G(N, 0.5)$ and $G(N, 0)$ as the convergent distributions. $G(N, 0)$ exhibits better generative performance than $G(N, 0.5)$.

G.3. Full results on graph generation tasks

We provide the mean and the standard derivation of metrics reported in the generic graph generation and large network generation tasks in Table 10 and Table 11, respectively.

Community					
	Structure-based metrics (MMD)			Neural-based metrics	
	Deg.	Clus.	Orb.	FID	RBF MMD
GRNN	0.1440 ± 0.0025	0.0535 ± 0.0264	0.0198 ± 0.0003	8.3869 ± 1.5429	0.1591 ± 0.0104
GRAN	0.1022 ± 0.0185	0.0894 ± 0.0082	0.0198 ± 0.0005	64.1145 ± 12.0927	0.0749 ± 0.0097
GraphCNF	0.1129 ± 0.0295	1.2882 ± 0.1918	0.0197 ± 0.0005	29.1526 ± 3.1900	0.1341 ± 0.0241
GDSS	0.0535 ± 0.0095	0.2072 ± 0.0520	0.0196 ± 0.0003	6.5531 ± 0.9418	0.0443 ± 0.0058
DiscDDPM	0.1238 ± 0.0068	0.6549 ± 0.0463	0.0246 ± 0.0004	8.6321 ± 1.1961	0.0840 ± 0.0099
DiGress	0.0409 ± 0.0041	0.0167 ± 0.0169	0.0298 ± 0.0002	3.4261 ± 0.4549	0.0460 ± 0.0069
EDGE	0.0175 ± 0.0056	0.0689 ± 0.0197	0.0198 ± 0.0002	2.2378 ± 0.5111	0.0227 ± 0.0097

Ego					
	Structure-based metrics (MMD)			Neural-based metrics	
	Deg.	Clus.	Orb.	FID	RBF MMD
GRNN	0.0768 ± 0.0142	1.1456 ± 0.0910	0.1087 ± 0.0442	90.5655 ± 19.2041	0.6827 ± 0.1181
GRAN	0.5778 ± 0.1415	0.3360 ± 0.0948	0.0406 ± 0.0112	489.9598 ± 42.1109	0.2633 ± 0.0911
GraphCNF	0.1010 ± 0.0421	0.7654 ± 0.0510	0.0820 ± 0.0334	18.7929 ± 3.5102	0.0896 ± 0.0125
GDSS	0.8189 ± 0.0691	0.6032 ± 0.2114	0.3315 ± 0.0591	60.6100 ± 8.1208	0.4331 ± 0.0982
DiscDDPM	0.4613 ± 0.1042	0.1681 ± 0.0735	0.0633 ± 0.0156	42.7994 ± 5.6312	0.1561 ± 0.0224
DiGress	0.0708 ± 0.0127	0.0092 ± 0.0062	0.1205 ± 0.0669	18.6794 ± 4.6395	0.0489 ± 0.0232
EDGE	0.0579 ± 0.0101	0.1773 ± 0.0521	0.0519 ± 0.0216	15.7614 ± 2.5021	0.0658 ± 0.0199

Table 10. Generation performance on generic graphs with standard derivation.

G.4. Visualizations

Visualization of generated generic graphs. We visualize six generic graphs from the test data and the generated graphs for each dataset in Figure 7 and 8. The visualized graphs are randomly selected from the test data and the generated samples.

Visualization of generated molecules. We visualize 16 molecules generated from GDSS, DiGress, and our approach in Figure 9.

Polblogs						
	EO	PLE	NTC	CC	CPL	AC
TRUE	100	1.414	1	0.226	2.736	-0.221
OPB	24.5 ± 0.4	1.395 ± 0.002	0.667 ± 0.013	0.150 ± 0.001	2.524 ± 0.005	-0.143 ± 0.003
HDOP	16.4 ± 0.3	1.393 ± 0.003	0.687 ± 0.021	0.153 ± 0.002	2.522 ± 0.009	-0.131 ± 0.006
CELL	26.8 ± 0.2	1.385 ± 0.001	0.810 ± 0.011	0.211 ± 0.002	2.536 ± 0.006	-0.230 ± 0.002
CO	20.1 ± 0.2	1.975 ± 0.107	0.045 ± 0.002	0.028 ± 0.001	2.502 ± 0.008	0.068 ± 0.009
TSVD	32.0 ± 0.2	1.373 ± 0.001	0.872 ± 0.023	0.205 ± 0.004	2.533 ± 0.005	-0.216 ± 0.005
VGAE	3.6 ± 0.2	1.723 ± 0.010	0.05 ± 0.006	0.001 ± 0.001	2.531 ± 0.063	-0.086 ± 0.009
GRNN	9.6 ± 0.5	1.334 ± 0.013	0.355 ± 0.048	0.095 ± 0.008	2.566 ± 0.056	0.096 ± 0.065
EDGE	16.5 ± 0.3	1.398 ± 0.002	0.977 ± 0.079	0.217 ± 0.005	2.647 ± 0.028	-0.214 ± 0.015
Cora						
	EO	PLE	NTC	CC	CPL	AC
TRUE	100	1.885	1	0.090	6.311	-0.071
OPB	10.9 ± 0.2	1.852 ± 0.008	0.097 ± 0.019	0.008 ± 0.001	4.476 ± 0.046	-0.037 ± 0.009
HDOP	0.9 ± 0.1	1.849 ± 0.011	0.113 ± 0.003	0.009 ± 0.001	4.477 ± 0.030	-0.030 ± 0.004
CELL	10.3 ± 0.2	1.774 ± 0.001	0.009 ± 0.003	0.002 ± 0.001	5.799 ± 0.012	-0.018 ± 0.013
CO	9.7 ± 0.5	1.776 ± 0.007	0.009 ± 0.002	0.002 ± 0.000	5.653 ± 0.044	0.010 ± 0.012
TSVD	6.7 ± 0.2	1.858 ± 0.012	0.349 ± 0.029	0.028 ± 0.001	4.908 ± 0.052	-0.006 ± 0.005
VGAE	1.5 ± 0.5	1.717 ± 0.005	0.120 ± 0.012	0.220 ± 0.012	4.934 ± 0.069	0.002 ± 0.010
GRNN	0.4 ± 0.1	1.822 ± 0.008	0.043 ± 0.007	0.011 ± 0.002	6.146 ± 0.065	0.043 ± 0.025
EDGE	0.9 ± 0.0	1.755 ± 0.005	0.446 ± 0.029	0.034 ± 0.002	4.995 ± 0.048	-0.046 ± 0.008
Road-Minnesota						
	EO	PLE	NTC	CC	CPL	AC
TRUE	100	2.147	1	0.028	35.349	-0.187
OPB	29.7 ± 0.3	2.188 ± 0.016	0.083 ± 0.036	0.002 ± 0.001	8.036 ± 0.051	0.009 ± 0.011
HDOP	13.2 ± 1.1	2.192 ± 0.065	0.208 ± 0.111	0.004 ± 0.001	8.274 ± 0.032	-0.024 ± 0.006
CELL	30.7 ± 1.3	2.267 ± 0.011	0.053 ± 0.069	0.001 ± 0.001	10.219 ± 0.096	-0.082 ± 0.004
CO	19.8 ± 0.9	2.044 ± 0.049	2.845 ± 0.916	0.040 ± 0.003	11.478 ± 0.075	-0.012 ± 0.008
TSVD	19.4 ± 0.6	2.172 ± 0.041	0.060 ± 0.046	0.001 ± 0.000	8.431 ± 0.130	0.006 ± 0.009
VGAE	1.3 ± 0.3	1.678 ± 0.091	0.096 ± 0.031	0.009 ± 0.001	11.120 ± 0.075	-0.027 ± 0.001
GRNN	0.6 ± 0.1	1.570 ± 0.017	0.099 ± 0.023	0.007 ± 0.002	11.695 ± 0.059	0.006 ± 0.009
EDGE	0.8 ± 0.1	1.910 ± 0.023	0.962 ± 0.101	0.011 ± 0.001	9.125 ± 0.088	-0.063 ± 0.006
PPI						
	EO	PLE	NTC	CC	CPL	AC
TRUE	100	1.462	1	0.092	3.095	-0.099
OPB	16.3 ± 0.2	1.443 ± 0.001	0.640 ± 0.007	0.058 ± 0.000	2.914 ± 0.005	-0.089 ± 0.003
HDOP	6.9 ± 0.1	1.444 ± 0.001	0.638 ± 0.007	0.058 ± 0.001	2.917 ± 0.008	-0.086 ± 0.003
CELL	6.7 ± 0.2	1.400 ± 0.000	0.248 ± 0.005	0.040 ± 0.001	3.108 ± 0.003	0.176 ± 0.004
CO	9.9 ± 0.1	1.754 ± 0.071	0.016 ± 0.001	0.006 ± 0.000	3.046 ± 0.002	0.043 ± 0.004
TSVD	13.2 ± 0.1	1.426 ± 0.001	0.848 ± 0.015	0.077 ± 0.001	2.867 ± 0.004	-0.089 ± 0.004
VGAE	0.5 ± 0.0	1.362 ± 0.006	0.091 ± 0.009	0.012 ± 0.005	2.991 ± 0.063	0.054 ± 0.007
GRNN	OOM	OOM	OOM	OOM	OOM	OOM
EDGE	7.5 ± 0.4	1.449 ± 0.003	0.981 ± 0.003	0.091 ± 0.031	3.028 ± 0.044	-0.107 ± 0.023

Table 11. Generation performance on large networks with standard derivation.

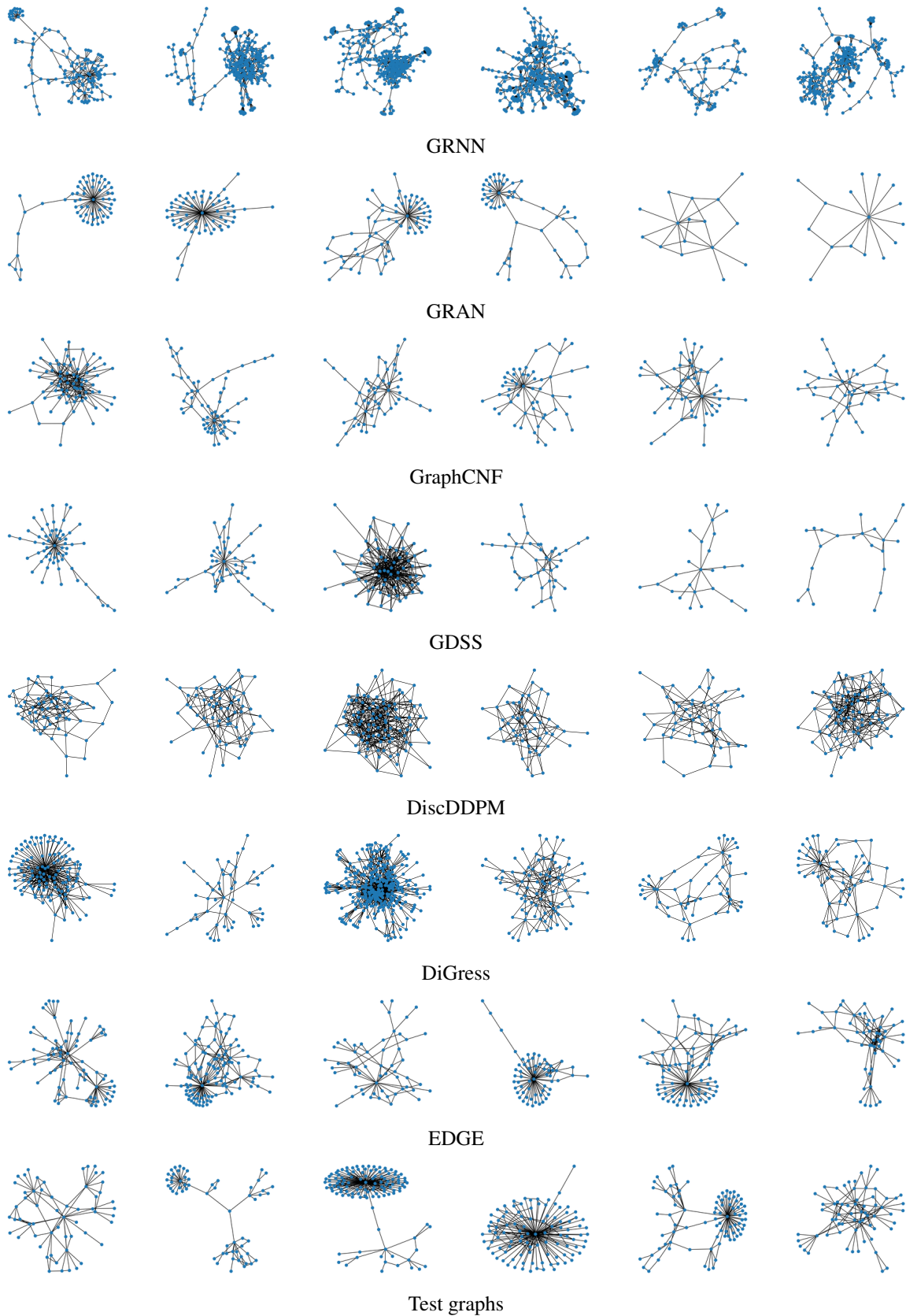


Figure 7. Visualization of the Ego dataset

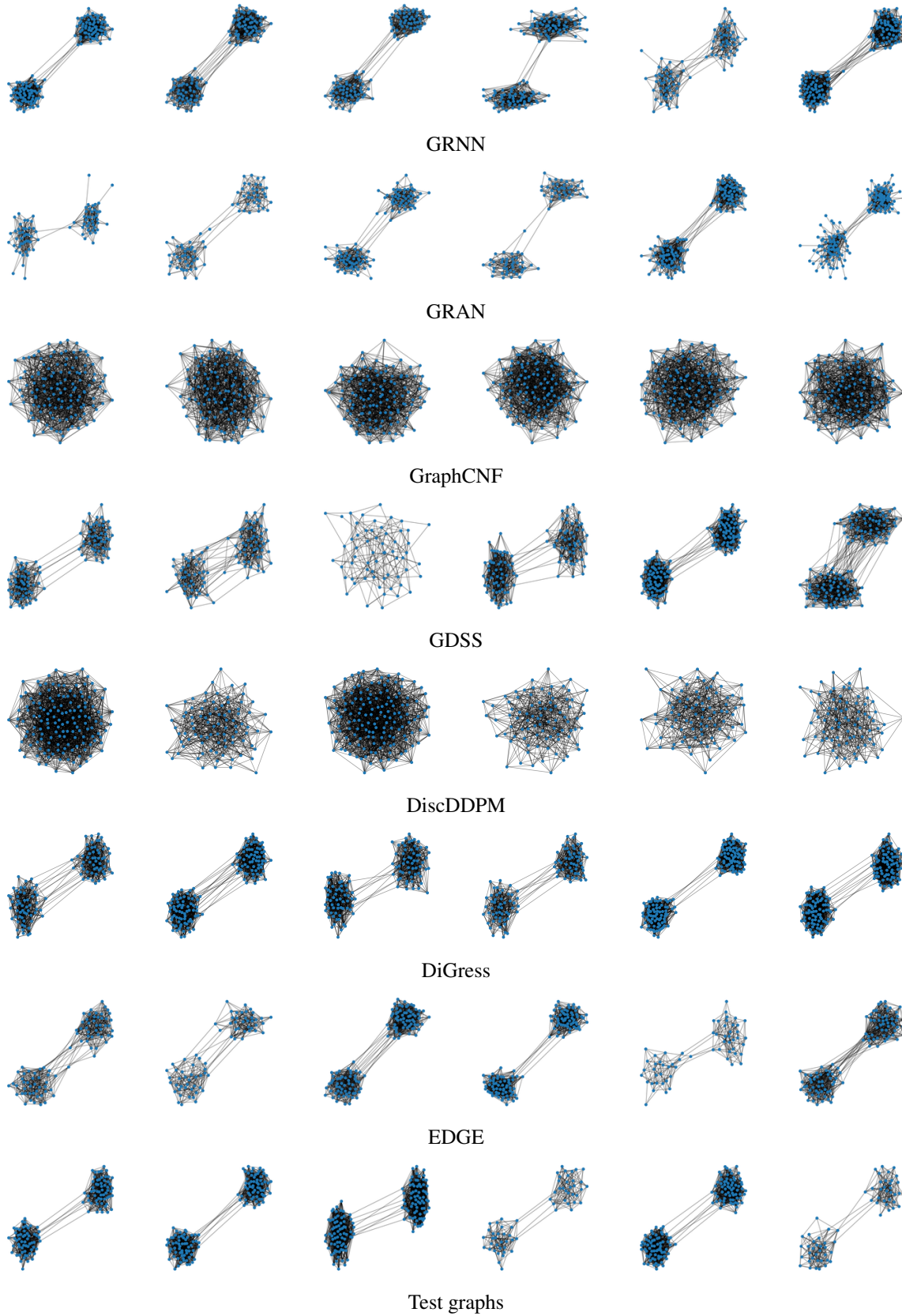


Figure 8. Visualization of the Community dataset

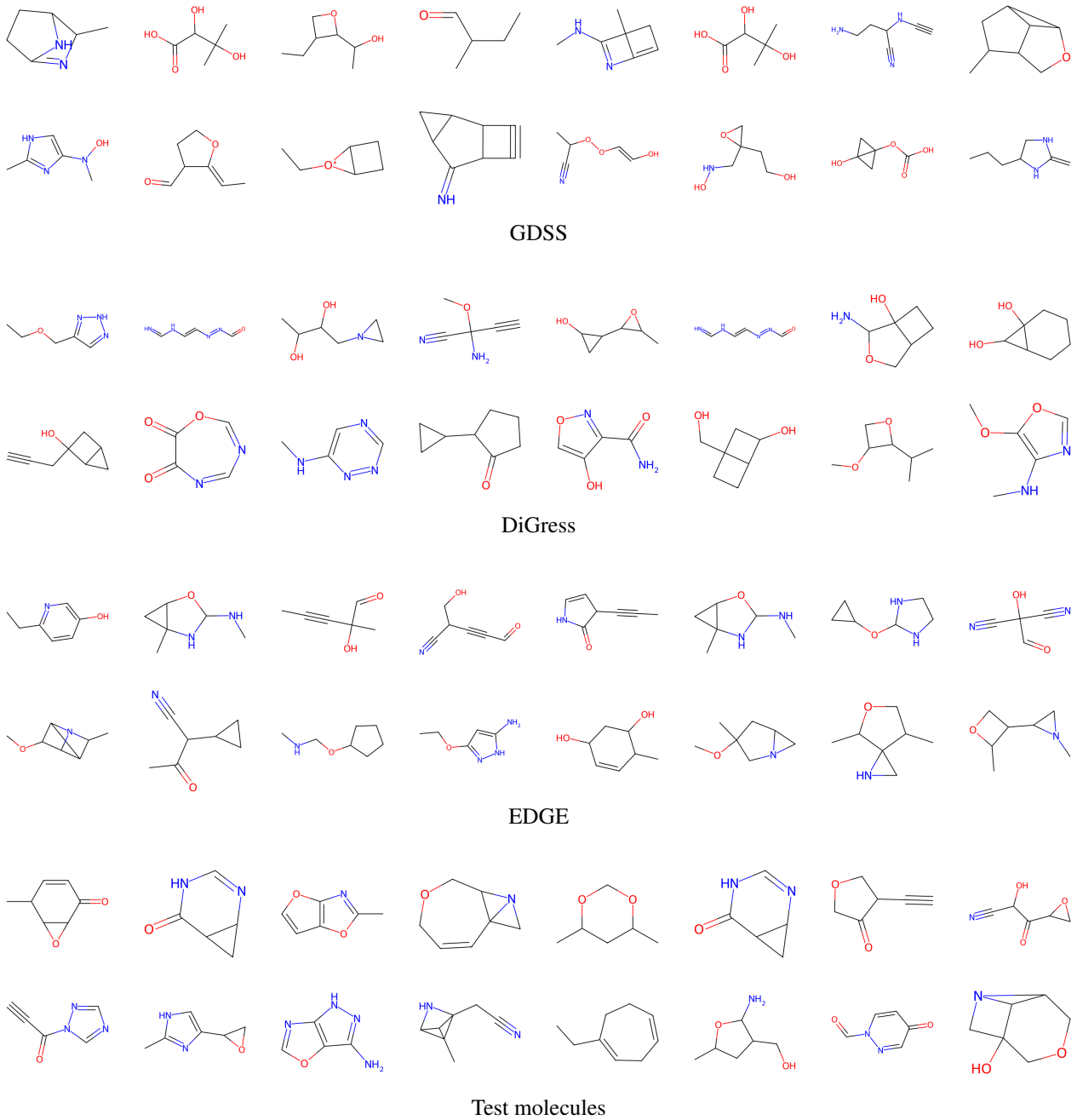


Figure 9. Visualization of the QM9 dataset